

# The Global Canopy Atlas: analysis-ready maps of 3D structure for the world's woody ecosystems

Fabian Jörg Fischer<sup>1 2</sup>, Becky Morgan<sup>1</sup>, Toby Jackson<sup>1</sup>, Jérôme Chave<sup>3</sup>, David Coomes<sup>4</sup>, KC Cushman<sup>5</sup>, Ricardo Dalagnol<sup>6</sup>, Michele Dalponte<sup>7</sup>, Laura Duncanson<sup>8</sup>, Sassan Saatchi<sup>9 6 10</sup>, Rupert Seidl<sup>11</sup>, Krzysztof Stereńczak<sup>12</sup>, Gaia Vaglio Laurin<sup>13</sup>, Stephen Adu-Bredu<sup>14 15</sup>, Jesús Aguirre-Gutiérrez<sup>16 17</sup>, Benedetta Antonielli<sup>18</sup>, John David Armston<sup>8</sup>, Mauro LR de Assis<sup>19</sup>, Nicolas Barbier<sup>20</sup>, Andrew Burt<sup>21</sup>, Ricardo Gomes César<sup>22</sup>, Jaroslav Cervenka<sup>23</sup>, Nicholas Coops<sup>24</sup>, Laury Cullen<sup>25</sup>, James W Dalling<sup>26 27</sup>, Andrew Davies<sup>28</sup>, Miro Demol<sup>21</sup>, Jakob Ebenbeck<sup>29</sup>, Fabian Fassnacht<sup>30</sup>, Lola Fatoyinbo<sup>31</sup>, Mariano García<sup>32</sup>, N. Ignacio Gasparri<sup>33 34</sup>, Terje Gobakken<sup>35</sup>, Tristan R.H. Goodbody<sup>24</sup>, Eric Bastos Görgens<sup>36</sup>, Tolga Gorum<sup>37</sup>, Carl Gosper<sup>38</sup>, Hongcan Guan<sup>39 40</sup>, Janne Heiskanen<sup>41 42</sup>, Marco Heurich<sup>29 43 44</sup>, Martina Hobi<sup>45</sup>, Bernhard Höfle<sup>46 47</sup>, Al Hooijer<sup>48</sup>, Andreas Huth<sup>49 50 51</sup>, Alexander Kedrov<sup>52</sup>, James R Kellner<sup>53 54</sup>, Simon Koenig<sup>29 43 55</sup>, Kamil Král<sup>56</sup>, Misha Krassovski<sup>57</sup>, Helga Kuechly<sup>58</sup>, Martin Krůček<sup>56</sup>, Kyaw Kyaw Htoo<sup>59</sup>, Nicolas Labrière<sup>60</sup>, Daphne Lai<sup>61</sup>, Johannes Larson<sup>62</sup>, Hjalmar Laudon<sup>62</sup>, Dawn Lemke<sup>63</sup>, Jonathan Lenoir<sup>64</sup>, Yadvinder Malhi<sup>65 66</sup>, Owais Ahmed Malik<sup>61</sup>, Maxence Martin<sup>67</sup>, Iain McNicol<sup>68</sup>, Milutin Milenkovic<sup>69</sup>, David Minor<sup>8</sup>, Ed Mitchard<sup>70 68</sup>, Vítězslav Moudrý<sup>71</sup>, Helene C. Muller-Landau<sup>72</sup>, Erik Næsset<sup>35</sup>, Anuttara Nathalang<sup>73</sup>, Jean Pierre Ometto<sup>19</sup>, Masanori Onishi<sup>59 74</sup>, Yusuke Onoda<sup>59</sup>, Petri Pellikka<sup>41 75</sup>, Henrik Persson<sup>76</sup>, Matheus Pinheiro Ferreira<sup>77</sup>, Pierre Ploton<sup>20</sup>, Suzanne M Prober<sup>78</sup>, Farhadur Rahman<sup>59 79</sup>, Parvez Rana<sup>80</sup>, Maxime Réjou-Méchain<sup>20</sup>, Jannika Schäfer<sup>81</sup>, Cornelius Senf<sup>82 83</sup>, Aurélie Shapiro<sup>84 85</sup>, Dmitry Schepaschenko<sup>86</sup>, Guochun Shen<sup>87 88</sup>, Miles Silman<sup>89 90</sup>, Thiago Silva<sup>91</sup>, Jenia Singh<sup>28</sup>, Ferry Slik<sup>92</sup>, Jonas Stillhard<sup>93</sup>, Anto Subash<sup>69</sup>, Ryuichi Takeshige<sup>59 94</sup>, Shengli Tao<sup>95 96</sup>, Evan Tenorio<sup>97</sup>, Timo Tokola<sup>98</sup>, Piotr Tompalski<sup>99</sup>, Nithin Tripathi<sup>100</sup>, Ruben Valbuena<sup>76</sup>, Riccardo Valentini<sup>101</sup>, Ronald Vernimmen<sup>48</sup>, Greg Vincent<sup>20</sup>, Jörgen Wallerman<sup>76</sup>, Wan Shafrina Wan Mohd Jaafar<sup>102</sup>, Yongcai Wang<sup>103</sup>, Hannah Weiser<sup>46 47</sup>, Joanne White<sup>99</sup>, Lukas Winiwarter<sup>46 104</sup>, Michael Wulder<sup>99</sup>, Zuoqiang Yuan<sup>105 106</sup>, Katherine Zdunic<sup>38</sup>, Yelu Zeng<sup>107 108</sup>, Houxi Zhang<sup>109</sup>, Jian Zhang<sup>110</sup>, Zhiming Zhang<sup>111</sup> and Tommaso Jucker<sup>1</sup>

## Affiliations

<sup>1</sup>School of Biological Sciences, University of Bristol, Bristol, BS8 1TQ United Kingdom

<sup>2</sup>Technical University of Munich, School of Life Sciences, Ecosystem Dynamics and Forest Management, Hans-Carl-von-Carlowitz-Platz 2, 85354 Freising, Germany

<sup>3</sup>Centre de Recherche Biodiversité Environnement, UMR 5300 (CNRS/IRD/Univ. Toulouse/INPT), Université de Toulouse, 31062 Toulouse Cedex 9, France

<sup>4</sup>Department of Plant Sciences, University of Cambridge, Cambridge, CB2 3EA, UK

<sup>5</sup>Oak Ridge National Laboratory (ORNL), Oak Ridge, TN (United States)

<sup>6</sup>Ctrees, Pasadena, CA, United States

<sup>7</sup>Research and Innovation Centre, Fondazione Edmund Mach, via E. Mach 1, 38098 San Michele all'Adige (TN), Italy

<sup>8</sup>University of Maryland, College Park, 2181 Lefrak Hall, College Park, Maryland 20742, USA

<sup>9</sup>Jet Propulsion Laboratory, California Institute of Technology, Pasadena, CA, United States

<sup>10</sup>Center for Tropical Research, Institute of the Environment and Sustainability, University of California Los Angeles, Los Angeles, CA, United States

<sup>11</sup>Berchtesgaden National Park, Doktorberg 6, 83471 Berchtesgaden, Germany

<sup>12</sup>Forest Research Institute, Braci Leśnej 3 Street, Sękocin Stary, 05-090 Raszyn, Poland

<sup>13</sup>Italian National Research Council, Research Institute on Terrestrial Ecosystems, Montelibretti Research Area, Italy

<sup>14</sup>Council for Scientific and Industrial Research (CSIR), Forestry Research Institute of Ghana, Kumasi, Ghana

<sup>15</sup>Department of Natural Resources Management, CSIR College of Science and Technology, Kumasi, Ghana

<sup>16</sup>Environmental Change Institute, School of Geography and the Environment, University of Oxford, Oxford, UK

<sup>17</sup>Leverhulme Centre for Nature Recovery, University of Oxford, Oxford, UK

<sup>18</sup>Serco Italia S.p.A., Via Bernardino Alimena 111-119, 00173, Rome (Italy).

<sup>19</sup>Coordenação Geral de Ciências da Terra, Instituto Nacional de Pesquisas Espaciais, São José dos Campos, SP, Brazil

<sup>20</sup>AMAP, Univ Montpellier, IRD, CNRS, INRAE, CIRAD, 34398 Montpellier cedex 5, France

<sup>21</sup>Sylvera Ltd, London, UK

<sup>22</sup>IPÊ Instituto de Pesquisas Ecológicas, Brazil

<sup>23</sup>Department of Nature Protection, Šumava National Park Administration, 1. máje 260, 38501 Vimperk, Czech Republic

<sup>24</sup>Integrated Remote Sensing Studio, Department of Forest Resources Management, University of British Columbia, 2424 Main Mall, Vancouver, BC, V6T 1Z4 Canada

<sup>25</sup>IPE-Instituto de Pesquisas Ecológicas, Rod. Dom Pedro I, km 47 Caixa Postal 47 12960-000 Nazaré, Paulista, SP, Brazil

<sup>26</sup>Department of Plant Biology, University of Illinois, Urbana-Champaign, Urbana, IL, 61801 USA

<sup>27</sup>Smithsonian Tropical Research Institute, Apartado 0843-03092, Balboa, Ancon, Panama

<sup>28</sup>Department of Organismic and Evolutionary Biology, Harvard University, 22 Divinity Avenue, Cambridge, MA 02138, USA

<sup>29</sup>Bavarian Forest National Park, Freyunger Straße, 94481 Grafenau, Germany

<sup>30</sup>Remote Sensing and Geoinformatics, Freie Universität Berlin, Malteserstraße 74-100, 12249 Berlin, Germany

<sup>31</sup>NASA Goddard Space Flight Center, 8800 Greenbelt Rd, Greenbelt, MD 20771, USA

<sup>32</sup>Universidad de Alcalá, Departamento de Geología, Geografía y Medio Ambiente, Environmental Remote Sensing Research Group, 28801, Alcalá de Henares, Spain

<sup>33</sup>Instituto de Ecología Regional (IER), Universidad Nacional de Tucumán-CONICET

<sup>34</sup>Facultad de Ciencias Naturales e IML- Universidad Nacional de Tucumán

<sup>35</sup>Norwegian University of Life Sciences, P.O. Box 5003, NMBU, 1432 Ås, Norway

<sup>36</sup>Departamento de Engenharia Florestal, Universidade Federal dos Vales do Jequitinhonha e Mucuri, Diamantina, MG, Brazil

<sup>37</sup>Eurasia Institute of Earth Sciences, Istanbul Technical University, Istanbul, Türkiye

<sup>38</sup>Biodiversity and Conservation Science, Department of Biodiversity, Conservation and Attractions, Kensington, WA 6151, Australia

<sup>39</sup>School of Ecology, Hainan University, Haikou 570228, China

<sup>40</sup>Collaborative Innovation Center of Ecological Civilization, Hainan University, Haikou 570228, China

<sup>41</sup>Department of Geosciences and Geography, University of Helsinki, P.O. Box 64, 00014 Helsinki, Finland

<sup>42</sup>Finnish Meteorological Institute, P.O. Box 503, 00101 Helsinki, Finland

<sup>43</sup>University of Freiburg, Tennenbacher Straße 2, 79106 Freiburg, Germany

<sup>44</sup>Department of Forestry and Wildlife Management, Inland Norway University of Applied Sciences, Koppang, Norway

<sup>45</sup>Swiss Federal Institute for Forest, Snow and Landscape Research WSL, Zürcherstrasse 111, 8903 Birmensdorf, Switzerland

<sup>46</sup>3DGeo Research Group, Institute of Geography, Heidelberg University, Im Neuenheimer Feld 368, 69120 Heidelberg, Germany

<sup>47</sup>Interdisciplinary Center for Scientific Computing (IWR), Heidelberg University, Im Neuenheimer Feld 205, 69120 Heidelberg, Germany

<sup>48</sup>Data for Sustainability, Axel, The Netherlands

<sup>49</sup>Helmholtz Centre for Environmental Research - UFZ, Permoserstr. 15, 04318 Leipzig, Germany

<sup>50</sup>University of Osnabrück, Barbarastr 12, D - 49076 Osnabrück, Germany

<sup>51</sup>German Centre for Integrative Biodiversity Research (iDiv), Puschstrasse 4, 04103 Leipzig, Germany

<sup>52</sup>Space Technologies and Services Center, Ltd, Perm, Russia

<sup>53</sup>Institute at Brown for Environment and Society, Brown University, Providence, RI 02912, USA

<sup>54</sup>Department of Ecology, Evolution and Organismal Biology, Brown University, Providence, RI 02912, USA

<sup>55</sup>German Space Agency at DLR, Königswinterer Straße 522-524, 53227 Bonn, Germany

<sup>56</sup>Department of Forest Ecology, Landscape Research Institute, Lidická 25/27, 602 00 Brno, Czech Republic

<sup>57</sup>Oak Ridge National Laboratory, Environmental Science Division, Oak Ridge, USA

<sup>58</sup>World Wide Fund for Nature (WWF) Germany

<sup>59</sup>Graduate School of Agriculture, Kyoto University, Kyoto, Japan

<sup>60</sup>Univ Toulouse, Toulouse INP, CNRS, IRD, Centre de Recherche sur la Biodiversité et l'Environnement (CRBE), Toulouse, France

<sup>61</sup>School of Digital Science, Universiti Brunei Darussalam, Jalan Tungku Link, Gadong, BE1410, Brunei Darussalam

<sup>62</sup>Department of Forest Ecology and Management, Swedish University of Agricultural Sciences, SLU Skogsmarksgränd 17, SE-901 83 Umeå, Sweden

<sup>63</sup>Department of Natural Resources and Environmental Sciences, Alabama A&M University, Normal, AL 35762, USA

<sup>64</sup>UMR CNRS 7058 « Ecologie et Dynamique Des Systèmes Anthropisés » (EDYSAN), Université de Picardie Jules Verne, Amiens Cedex, France

<sup>65</sup>Environmental Change Institute, School of Geography and the Environment, University of Oxford, South Parks Road, United Kingdom

<sup>66</sup>Leverhulme Centre for Nature Recovery, University of Oxford, South Parks Road, United Kingdom

<sup>67</sup>Institut de Recherche sur les Forêts, Université du Québec en Abitibi-Témiscamingue, Québec, Canada

<sup>68</sup>School of GeoSciences, University of Edinburgh, Alexander Crum Brown Road, Edinburgh, EH9 3FF, UK

<sup>69</sup>Novel Data Ecosystems for Sustainability (NoDES) Research Group, Advancing Systems Analysis Program, International Institute for Applied Systems Analysis (IIASA), Laxenburg, Austria

<sup>70</sup>Space Intelligence, 93 George Street, Edinburgh EH2, 3ES, UK

<sup>71</sup>Department of Spatial Sciences, Faculty of Environmental Sciences, Czech University of Life Sciences Prague, Praha-Suchbát, Czech Republic

<sup>72</sup>Smithsonian Tropical Research Institute, Balboa, Panama

<sup>73</sup>National Biobank of Thailand, National Science and Technology Development Agency, Pathum Thani, 12120, Thailand

<sup>74</sup>DeepForest Technologies Co., Ltd., Kyoto, Japan

<sup>75</sup>State Key Laboratory of Information Engineering in Surveying, Mapping and Remote Sensing, Wuhan University, Wuhan 430072, China

<sup>76</sup>Department of Forest Resource Management, Swedish University of Agricultural Sciences, SLU Skogsmarksgränd 17, SE-901 83 Umeå, Sweden

<sup>77</sup>Dept. of Forest Sciences, 'Luiz de Queiroz' College of Agriculture (ESALQ), University of São Paulo (USP)

<sup>78</sup>CSIRO Environment, Canberra, ACT 2601, Australia

<sup>79</sup>Department of Remote Sensing and GIS, Bangabandhu Sheikh Mujibur Rahman Agricultural University, Gazipur, Dhaka, Bangladesh

<sup>80</sup>Natural Resources Institute Finland (Luke), Latokartanonkaari 9, Helsinki, 00790, Finland

<sup>81</sup>Institute of Geography and Geoecology (IFGG), Karlsruhe Institute of Technology (KIT), Kaiserstraße 12, 76131 Karlsruhe, Germany

<sup>82</sup>Technical University of Munich, School of Life Sciences, Earth Observation for Ecosystem Management, Hans-Carl-von-Carlowitz-Platz 2, 85354 Freising, Germany

<sup>83</sup>Munich Data Science Institute

<sup>84</sup>Food & Agriculture Organization of the United Nations (FAO)

<sup>85</sup>Here+There Mapping Solutions

<sup>86</sup>International Institute for Applied Systems Analysis (IIASA) Schlossplatz 1, 2361 Laxenburg, Austria.

<sup>87</sup>Zhejiang Tiantong Forest Ecosystem National Observation and Research Station, School of Ecological and Environmental Sciences, East China Normal University, Shanghai 200241, China

<sup>88</sup>Shanghai Institute of Pollution Control and Ecological Security, Shanghai 200092, China

<sup>89</sup>Department of Biology, Wake Forest University, Winston-Salem, North Carolina, USA

<sup>90</sup>The Sabin Center for Environment and Sustainability, Wake Forest University, Winston-Salem, North Carolina, USA

<sup>91</sup>Biological and Environmental Sciences, University of Stirling, Stirling, UK

<sup>92</sup>Environmental and Life Sciences, Faculty of Science, Universiti Brunei Darussalam, Gadong, Brunei Darussalam

<sup>93</sup>Swiss Federal Institute for Forest, Snow, and Landscape Research WSL, 8903 Birmensdorf, Switzerland

<sup>94</sup>Biodiversity Division, National Institute for Environmental Studies, Tukuba, Ibaraki, Japan

<sup>95</sup>Institute of Ecology, College of Urban and Environmental Sciences, and State Key Laboratory of Vegetation Structure, Function and Construction (VegLab), Peking University, Beijing 100871, China.

<sup>96</sup>State Key Laboratory for Vegetation Structure, Function and Construction (VegLab), Peking University, Beijing 100871, China

<sup>97</sup>Alabama A&M University, Normal, AL 35762, USA

<sup>98</sup>School of Forest Sciences, University of Eastern Finland, Joensuu, FIN-80100, Finland

<sup>99</sup>Canadian Forest Service, Natural Resources Canada, 506 West Burnside Road, Victoria, BC V8Z 1M5, Canada

<sup>100</sup>Asian Institute of Technology, School of Engineering and Technology, P.O.Box 4, Klong Luang, Pathumthani 12120, Thailand

<sup>101</sup>Department for Innovation in Biological, Agro-food, and Forestry Systems, Tuscia University, Viterbo, Italy

<sup>102</sup>Earth Observation Centre, Institute of Climate Change, Universiti Kebangsaan Malaysia, 43600 Selangor, Malaysia

<sup>103</sup>Center for Satellite Application on Ecology and Environment, Ministry of Ecology and Environment, Beijing, 100094, China

<sup>104</sup>Unit of Geometry and Surveying, Faculty of Engineering Sciences, University of Innsbruck, 6020 Innsbruck, Austria

<sup>105</sup>Shaanxi Key Laboratory of Qinling Ecological Intelligent Monitoring and Protection, School of Ecology and Environment, Northwestern Polytechnical University, China

<sup>106</sup>CAS Key Laboratory of Forest Ecology and Management, Institute of Applied Ecology, Chinese Academy of Sciences, Shenyang, China

<sup>107</sup>College of Land Science and Technology, China Agricultural University, Beijing 100083, China

<sup>108</sup>Key Laboratory of Remote Sensing for Agri-Hazards, Ministry of Agriculture and Rural Affairs, Beijing 100083, China

<sup>109</sup>Forestry College, Fujian Agriculture and Forestry University, Fuzhou 350028, China

<sup>110</sup>State Key Laboratory of Biocontrol, School of Life Sciences, Sun Yat-sen University, Guangzhou, 510275 P.R. China

<sup>111</sup>State Key Laboratory of Vegetation Structure, Function and Construction (VegLab) and School of Ecology and Environmental Sciences, Yunnan University, 650091 Kunming, China

## 1 **Abstract**

2 Woody canopies regulate exchanges of energy, water and carbon, and their three-dimensional  
3 (3D) structure supports much of terrestrial biodiversity. Remote sensing technologies such as  
4 airborne laser scanning (ALS) now enable the 3D mapping of entire landscapes. However, we  
5 lack the large, harmonized and geographically representative ALS collections needed to build  
6 a global picture of woody ecosystem structure. To address this challenge, we developed the  
7 Global Canopy Atlas (GCA): 3,458 ALS acquisitions transformed into standardized and  
8 analysis-ready maps of canopy height and elevation at 1 m<sup>2</sup> resolution. The GCA covers  
9 56,554 km<sup>2</sup> across all major biomes. 19% of this area has been scanned multiple times, and  
10 87% of all GCA products are openly available, covering 95% of the total area. To showcase  
11 its wide range of applications, we applied the GCA in three case studies. First, we validated  
12 three global satellite-derived canopy height maps, finding poor performance at native  
13 resolution (1-30 m,  $R^2 < 0.38$ ) and moderate performance at 250 m resolution ( $R^2 < 0.65$ ).  
14 Second, analyzing global patterns in canopy gap size frequency we discovered an  
15 unexpectedly large variation of power law exponents from branch to stand level ( $\alpha = 1.52$  to  
16 2.38), pointing to a fundamental scale-dependence of forest structure. Third, we developed a  
17 framework to standardize forest turnover quantification from multi-source, multi-temporal ALS.  
18 In a temperate forest in North America it revealed that 21% of canopy gaps closed within 12  
19 years of opening and would thus be missed by infrequent monitoring. As demonstrated by  
20 these case studies, the GCA provides a novel data source for ecologists, foresters, remote  
21 sensing scientists and the ecosystem modelling community that substantially advances our  
22 ability to understand the structure and dynamics of woody ecosystems at global scales.

23

24

25 **Key words:** airborne laser scanning, ecosystem structure, digital terrain model, canopy  
26 height, satellite remote sensing, forest gaps, scaling law, disturbance, canopy closure

## 27 **1. Introduction**

28 Over the past two decades, airborne laser scanning (ALS) has become integral to the  
29 environmental sciences (Beland et al., 2019; Eitel et al., 2016). Laser pulses emitted from  
30 aircraft penetrate deep into vegetation canopies, and – by reflecting off leaves, branches and  
31 trunks – create a three-dimensional (3D) image of vegetation structure. This information is  
32 now routinely used for mapping forest resources (Fassnacht et al., 2024; Næsset et al., 2004),  
33 microclimates (Gril et al., 2023) and biodiversity (Davies & Asner, 2014; Toivonen et al., 2023).  
34 It is also central to the upscaling of vegetation properties such as aboveground carbon stocks  
35 (Asner et al., 2014; Coops et al., 2021; Ometto et al., 2023; Xu et al., 2017). At submetric  
36 accuracy, ALS reveals an ecological complexity that we are only just finding a language for  
37 (Atkins et al., 2023; Lines et al., 2022), and, with frequent, automated surveying on the horizon  
38 (Besson et al., 2022), it can help uncover the fundamental processes of how organisms,  
39 communities and their biomass develop in space and time (Battison et al., 2024; Jackson et  
40 al., 2024; Næsset et al., 2013). These insights will enable us to train a new generation of  
41 satellite monitoring tools (Kellogg et al., 2020; Quegan et al., 2019), calibrate high-resolution  
42 vegetation models (Fischer et al., 2020; Shugart et al., 2015), and shape conservation policies  
43 (Gonzalez et al., 2023). However, to build a comprehensive picture of the 3D structure and  
44 dynamics of ecosystems, we must move beyond single-time, single-site studies and  
45 harmonize ALS data and derivatives at global scales (Valbuena et al., 2020).

46 ALS data are increasingly available for this purpose. Most countries in Europe and  
47 North America now have substantial ALS coverage, with wall-to-wall acquisitions in many  
48 areas at regional scale or below (Moudrý et al., 2024; White et al., 2025), and facilities such  
49 as OpenTopography (<https://opentopography.org>), 3DEP ([https://www.usgs.gov/3d-elevation-](https://www.usgs.gov/3d-elevation-program)  
50 [program](https://www.usgs.gov/3d-elevation-program)) or ELVIS (<https://elevation.fsd.org.au>) consolidate ALS data from a wide range of  
51 sources in the United States, New Zealand and Australia. As an alternative to wall-to-wall  
52 coverage, targeted ALS campaigns have been employed to collect representative samples  
53 over large biomes (Wulder, White, Nelson, et al., 2012). Examples include the Amazon

54 (Ometto et al., 2023), the Congo Basin (Xu et al., 2017), Borneo (Melendy et al., 2018), Peru  
55 (Asner et al., 2014), and Canada’s boreal forests (Wulder, White, Bater, et al., 2012), as well  
56 as data-rich ecological “supersites” (Kampe, 2010; Karan et al., 2016; White et al., 2019).  
57 However, despite these advances, there is still a distinct lack of harmonization at global scales  
58 (Stereńczak et al., 2020). Three issues stand out in particular. First, the acquisition of ALS  
59 varies considerably across locations and projects. They are acquired in different seasons, with  
60 different instruments, at different altitudes, and often without consistent reporting standards –  
61 all of which can introduce substantial uncertainties into assessments of ecosystem 3D  
62 structure (Almeida et al., 2019; Fischer et al., 2024; Joerg et al., 2012; Næsset, 2005, 2009;  
63 Okyay et al., 2019; Riofrío et al., 2022; Roussel et al., 2017). Second, the processing of ALS  
64 data varies widely. It lacks minimum quality specifications and is carried out with different  
65 algorithms, for different aims, and often with little documentation. Ecologically relevant  
66 quantities such as canopy height, cover, and density can therefore come with errors that are  
67 difficult to correct for and make robust comparisons across studies difficult if not impossible  
68 (Fischer et al., 2024; Kissling & Shi, 2023; LaRue et al., 2022; Quan et al., 2021; Vincent et  
69 al., 2023; Zhang et al., 2024). Third, the accessibility of ALS data and derived products is  
70 inconsistent, with data provided in different formats, with varying data sharing policies and  
71 access protocols. It requires specialist knowledge and considerable time to find, download  
72 and harmonise ALS data, which substantially slows progress towards global syntheses.

73 To tackle these challenges, we here present the Global Canopy Atlas (GCA), a  
74 harmonised database of 3,458 ALS-derived maps of canopy height and elevation at 1 m<sup>2</sup>  
75 resolution, covering 56,554 km<sup>2</sup> of the world’s woody ecosystems. Its ALS samples have been  
76 processed using a harmonised pipeline designed to enable robust comparisons across  
77 acquisitions (Fischer et al., 2024). Products include several digital terrain models (DTMs,  
78 ground elevation), digital surface models (DSMs, total surface elevation), and canopy height  
79 models (CHMs, top canopy height), all delivered in an easy-to-share GeoTIFF format.  
80 Products are supplemented with a range of ancillary spatialized data quality layers and  
81 comprehensive metadata recording everything from acquisition dates, instrumentation, flight

82 specifications and geolocation. 87% of the GCA products will be made freely available through  
83 the European Space Agency's Multi-Mission Algorithm and Analysis Platform (MAAP),  
84 including thorough documentation and links to the original ALS data sources. In doing so, the  
85 GCA provides a novel resource for ecological research, global change studies, and the  
86 environmental sciences more broadly. Below, we describe its assembly and contents before  
87 demonstrating its range of applications through three case studies that focus on (1) the  
88 validation of global satellite-derived canopy height models, (2) global patterns in canopy gap  
89 size frequency, and (3) forest turnover quantification from multi-temporal ALS data.

## 90 **2. Database construction**

### 91 **2.1 Data aggregation**

92 To assemble the GCA, we searched and documented ALS acquisitions across the globe that  
93 could be converted into high-quality maps of terrain and canopy height. We employed a broad  
94 definition of ALS data, including acquisitions from airplanes and drones (fixed-wing and rotor-  
95 based). We did not include any form of terrestrial laser scanning (TLS) or mobile laser  
96 scanning (MLS).

97 We followed a number of guidelines during the assembly of the GCA. First, we put a  
98 focus on landscapes with natural woody vegetation cover, i.e., areas without large-scale  
99 human interventions such as urban and agricultural zones or plantations of introduced  
100 species. Second, we prioritised representativity and balanced sampling in geographical and  
101 environmental space. This means, when downloading data from publicly available ALS  
102 collections, we selected subsets covering areas of at least 1 km<sup>2</sup>, ideally 5-10 km<sup>2</sup>, a wide  
103 geographic range, and a diversity of ecosystem types. Third, we only included acquisitions  
104 where raw ALS data – so-called “point clouds” – were available, so that a standardized  
105 processing pipeline could be applied (Fischer et al., 2024). Fourth, we filtered data according  
106 to a set of minimum quality standards. These included a target sampling density of at least 2  
107 pulses m<sup>-2</sup> (based on metadata information), compliance with the LAS format standard  
108 ([https://www.asprs.org/wp-content/uploads/2019/07/LAS\\_1\\_4\\_r15.pdf](https://www.asprs.org/wp-content/uploads/2019/07/LAS_1_4_r15.pdf), last accessed on 26

109 August 2025), and the availability of metadata for flight configuration and acquisition dates.  
110 We also prioritised “leaf-on” over “leaf-off” acquisitions for ecosystems that are deciduous.  
111 This meant not including a wide range of openly available wall-to-wall ALS data, such as  
112 available through governmental agencies, as these are often insufficiently documented, low in  
113 pulse density or from winter acquisitions. We note, however, that these were broad guidelines.  
114 We made exceptions to improve geographic coverage, or to sample sites of particular  
115 ecological interest. Therefore, the GCA also includes acquisitions from heavily  
116 anthropogenically modified landscapes, with densities  $<2$  pulses  $m^{-2}$ , or with imprecise  
117 metadata on flight dates. Areal coverage can reach several 100  $km^2$  in national parks, but also  
118 go down to a few hectares for drone acquisitions.

119 Using these guidelines, we assembled the GCA from a wide range of sources. An  
120 overview over all datasets that we included is provided in Table S1. We downloaded open  
121 collections from dedicated ecosystem observatories such as the Brazilian Sustainable  
122 Landscapes program (<https://www.paisagenslidar.cnptia.embrapa.br/>, this and all following  
123 links accessed on 26 August 2025), the United States’ National Ecological Observatory  
124 Network (Kampe, 2010) and Australia’s Terrestrial Ecosystem Research Network (TERN,  
125 <http://portal.tern.org.au/>). We supplemented them with ALS campaigns such as the Estimativa  
126 de Biomassa na Amazônia (EBA) initiative ([https://www.ccst.inpe.br/projetos/eba-estimativa-  
127 de-biomassa-na-amazonia/](https://www.ccst.inpe.br/projetos/eba-estimativa-de-biomassa-na-amazonia/)), the World Wildlife Fund’s (WWF) acquisitions over the  
128 Democratic Republic of Congo (Xu et al., 2017) and individual research projects. We  
129 complemented targeted ALS acquisitions with openly available data from country-specific  
130 websites (e.g., <https://geoservices.ign.fr/lidarhd> in France) and collections such as  
131 OpenTopography, with a focus on protected areas and those with a low human footprint.  
132 Additionally, we contacted research groups who had acquired ALS data over large  
133 environmental gradients or at specific research sites (Stereńczak et al., 2020) and invited them  
134 to contribute to the database.

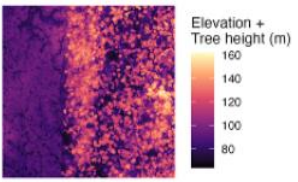
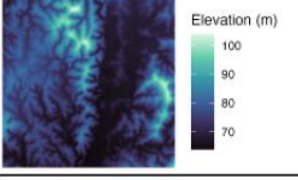
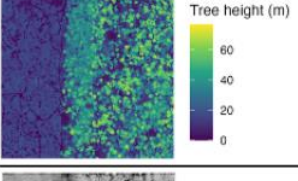
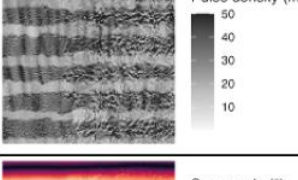
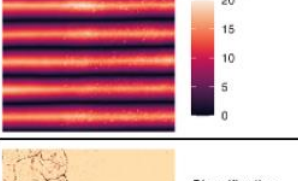

135

136

## 137 **2.2 Data processing and quality checks**

138 All data processing was carried out with the same standardized pipeline, which is described  
139 in detail in Fischer et al. (2024). The pipeline is fully automatic and based on a few key software  
140 tools, mainly the laser scanning software LAStools and the R packages data.table (Dowle &  
141 Srinivasan, 2025), terra (Hijmans, 2025), sf (Pebesma, 2018), and lidR (Roussel et al., 2020).  
142 It carries out several pre- and post-processing steps, such as the splitting of ALS data into  
143 coherent spatial units as well as noise filtering, deduplication, and ground classification. For  
144 each spatial unit, the output is a set of DTMs, DSMs, and CHMs, as well as several types of  
145 ancillary layers for quality control. For most applications, we recommend the default DTM and  
146 a CHM derived either from a triangulated irregular network (TIN) or a locally adaptive version  
147 of the spikefree algorithm (Khosravipour et al., 2016), both of which performed well in a  
148 robustness assessment (Fischer et al., 2024). An overview of the different types of layers  
149 generated by the pipeline is provided in Table 1, with further information in Table S2.

150 Throughout processing, we kept all parameters constant across ALS acquisitions, with  
151 only few manual adjustments. For example, pre-classified noise points (LAS class 7 and 18)  
152 were always excluded, but for some datasets we also excluded custom noise classes defined  
153 by the data providers. These noise classes reflected manual corrections of scan artefacts or  
154 dense noise that would not be captured by automatic noise detection. In terms of geolocation,  
155 our default approach was to retain any provided metric coordinate system to ensure  
156 consistency with metadata. However, if acquisitions were provided in imperial units (ft), we  
157 converted them into SI units and Universal Transverse Mercator (UTM) coordinates to ensure  
158 global comparability. The same approach – retaining the original data configuration where  
159 possible – was applied to vertical geo-referencing, so acquisitions were generally processed  
160 with the provided ellipsoid or geoid reference. While this does not affect woody ecosystem  
161 structure quantification (CHMs), there may be a location-dependent offset between ellipsoidal  
162 and geoidal datum up to around 100m (DTMs and DSMs).

| Map type                    | Products  | Description  | Example   |
|-----------------------------|---|--|---|
| Digital surface model (DSM) | <ul style="list-style-type: none"> <li>dsm_lspikefree.tif</li> <li>dsm_tin.tif</li> <li>dsm_highest.tif</li> </ul>  | Three maps of combined ground elevation and vegetation height at 1 m resolution. They reflect varying methods of interpolating top height. The default is a “spikefree” model (dsm_lspikefree.tif). The raster of highest laser returns (dsm_highest.tif) should be used cautiously, as it underestimates height in low-pulse density areas.                         |    |
| Digital terrain model (DTM) | <ul style="list-style-type: none"> <li>dtm.tif</li> <li>dtm_lasdef.tif</li> <li>dtm_supplied.tif</li> <li>dtm_lasfine.tif</li> <li>dtm_highest.tif</li> </ul> | Five maps of ground elevation at 1 m resolution, interpolated from ground returns. They reflect varying methods of classifying returns as ground and interpolating between them. The default (dtm.tif) builds on the standard ground classification algorithm of the LASools software but refines it on steep slopes ( $\geq 40^\circ$ ).                            |    |
| Canopy height model (CHM)   | <ul style="list-style-type: none"> <li>chm_lspikefree.tif</li> <li>chm_tin.tif</li> <li>chm_highest.tif</li> </ul>  | Three maps of vegetation height at 1 m resolution. Each CHM is derived from the corresponding DSM by subtracting the default DTM (dtm.tif).  |    |
| Pulse density               | <ul style="list-style-type: none"> <li>pulsedensity.tif</li> <li>pulsedensity_lastreturn.tif</li> <li>pulsedensity_scanangle20.tif</li> </ul>                 | Three maps of laser pulse density at 1 m resolution. They reflect different methods for pulse density inference (first returns, last returns, first returns with scan angles $< 20^\circ$ ). The default is first return density (pulsedensity.tif), which also includes single returns. Best aggregated to coarser resolution (5-10 m) to reduce small-scale noise. |   |
| Scan angle                  | <ul style="list-style-type: none"> <li>scanangle_abs.tif</li> </ul>   | One map of absolute scan angle at 1 m resolution. Reflects the mean scan angle of pulses that sampled a particular 1 m <sup>2</sup> pixel.   |  |
| Classification              | <ul style="list-style-type: none"> <li>classification_supplied.tif</li> </ul>   | One map of land classification at 1 m resolution. Only available if laser scans have been pre-classified by data provider. Reflects default lidar classes as defined in the LAS standard. If present, can be used to differentiate buildings (class 6) and rail or road surfaces (classes 10 and 11) from vegetation (classes 3 to 5).                               |  |

163

164 **Table 1: Overview of types of spatial layers provided as part of the Global Canopy Atlas.** For several of the  
 165 derived layers (e.g., CHMs and DTMs) we provide a range of alternative options generated using different  
 166 algorithms which are described in Table S2 and in Fischer et al. (2024). We briefly summarise these in the  
 167 description provided above and highlight the suggested default maps for most purposes. Sample data come from  
 168 a 2020 acquisition at the Sepilok Forest Reserve in Malaysian Borneo and show a 1 km<sup>2</sup> tile of where the reserve  
 169 (right) borders an oil palm plantation (left).

170

171 Data quality standards varied across data providers and instrumentation, with errors ranging  
 172 from negligible (isolated noise points) to considerable but repairable (faulty geolocation, flight  
 173 line misalignment) to substantial and beyond repair (insufficient canopy penetration or flight  
 174 line overlap). To process large numbers of ALS acquisitions, we developed automatic

175 procedures for quality assurance and control. The vast majority of these quality checks are  
176 directly embedded in the processing pipeline and provided as ancillary layers alongside the  
177 DTMs and CHMs (Table 1, Table S2). This gives users flexibility in choosing appropriate  
178 quality levels before and during data analysis. General quality layers include pulse density  
179 rasters that enable users to identify areas of poor sampling (pulsedensity.tif), derived pulse  
180 density masks (mask\_pd02.tif and mask\_pd04.tif, subsetting to regions with  $>2$  or 4 pulses  $m^{-2}$ ,  
181 respectively), rasterizations of scan angles (scanangle\_abs.tif), which enable identification  
182 of flightline patterns, as well as masks for potential high noise or cloud points (mask\_cloud.tif).  
183 In addition, we provide several alternative DTM layers to assess robustness of ground  
184 detection, which is a major source of uncertainty on steep slopes and under dense forest cover  
185 (Stereńczak et al., 2016), as it requires both dense sampling and high laser power. Users can  
186 investigate how and where DTMs disagree or use pre-computed DTM masks that highlight  
187 areas with high uncertainty (mask\_unstabledtm.tif) and those on steep slopes where features  
188 such as cliffs hamper robust ground classification (mask\_steep.tif).

189

### 190 **2.3 Processing reports**

191 Each processed acquisition is accompanied by an automatic two-page PDF processing report  
192 (Fig. S1, also provided as separate pdf in the Supplementary). The first page provides an  
193 informal quality check, showing the acquisition outline overlaid on local maps from  
194 OpenStreetMap and optical imagery from ESRI, downloaded via the R basemaps package  
195 (Schwalb-Willmann, 2024). The second page provides a more detailed and quantitative  
196 overview. It shows a pulse density rasterization where areas with pulse densities  $<2 m^{-2}$  are  
197 flagged to provide a rapid assessment of lower-quality scan areas, as well as a DTM reliability  
198 mask (mask\_unstabledtm.tif). It also shows the timing of the acquisition with respect to  
199 vegetation greenness/phenology (NDVI and EVI) and snow cover obtained from the MODIS  
200 Aqua and Terra sensors (Didan, 2025). Finally, the second page of the processing report also  
201 compares ALS-derived products with three satellite-derived layers: the Copernicus World  
202 DSM at 90 m resolution (European Space Agency, 2024), top canopy height (RH98) estimated

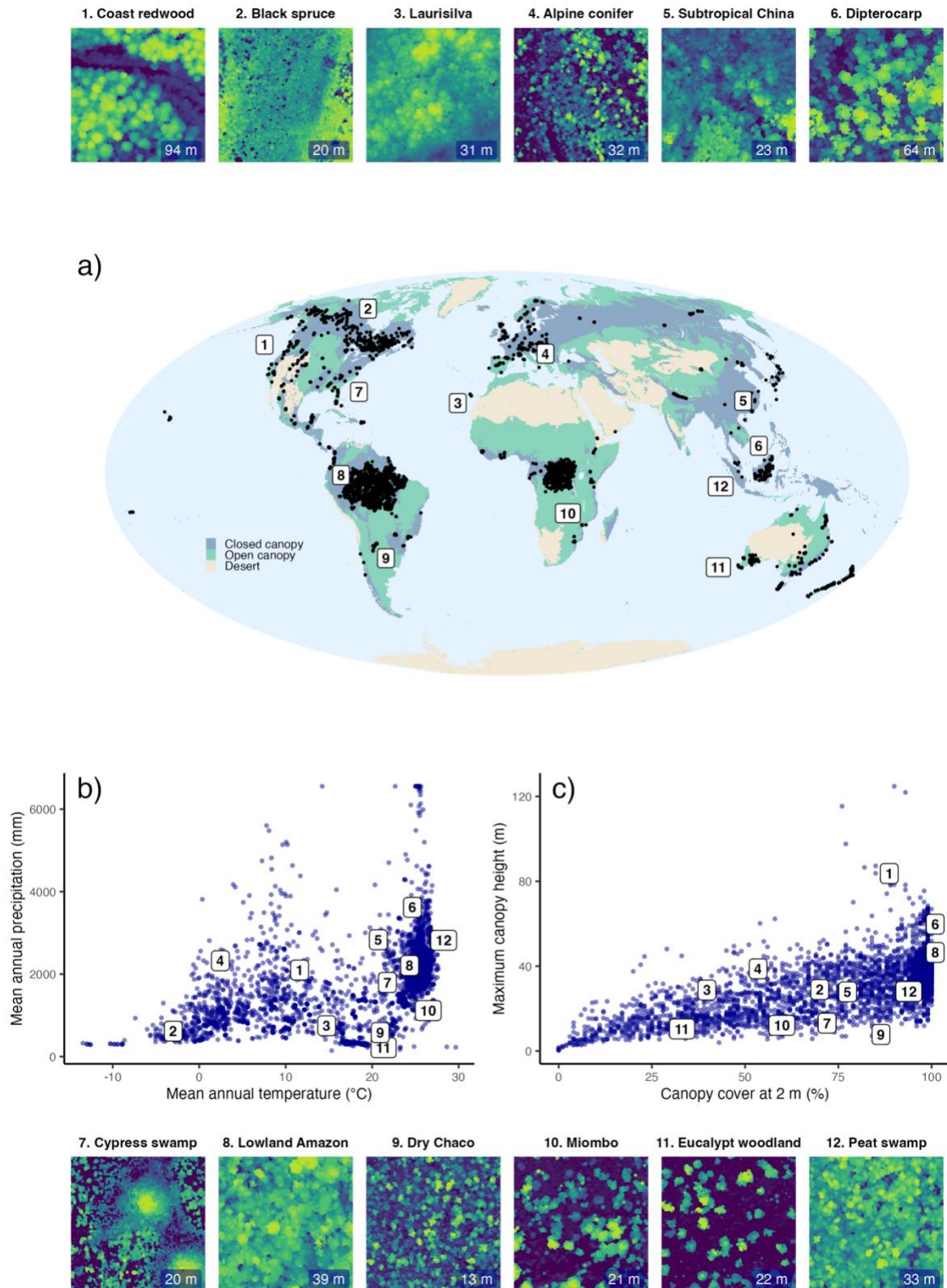
203 from GEDI/ICESat-2 at 100 m resolution (Saatchi & Favrichon, 2023), and global canopy  
204 height derived from Landsat at 30 m resolution (Potapov et al., 2022). ALS data provide more  
205 accurate representations of terrain and vegetation structure than satellites, but we have found  
206 the comparison useful for practical purposes. First, it helps identify potential geo-location  
207 errors. For example, correlations between ALS DSMs and the Copernicus World DSM are  
208 generally high ( $R^2 > 0.9$ ), so low correlations can indicate assignment to the wrong UTM zone  
209 or constant horizontal offsets. Second, the comparison also provides a quick indicator of how  
210 well common satellite products represent local vegetation structure, including temporal offsets,  
211 and thus offers an insight into upscaling opportunities, a key application of ALS data (Coops  
212 et al., 2021).

### 213 **3. Database overview**

214 The GCA database consists of 3,458 ALS acquisitions converted into maps of vegetation  
215 height and terrain elevation at 1 m<sup>2</sup> resolution (Fig. 1a). These acquisitions vary considerably  
216 in size from 0.1 to 203.7 km<sup>2</sup> (95% interval). The vast majority (85%) cover 1 km<sup>2</sup> or more, and  
217 the overall median area is 8.5 km<sup>2</sup>. All acquisitions together cover 56,554 km<sup>2</sup> of land area  
218 spread across 56 countries and 224 ecoregions (Dinerstein et al., 2017). About 57% of this  
219 area (31,554 km<sup>2</sup>) is in intact forest landscapes (Potapov et al., 2017) or has some form of  
220 protection designation (World Database of Protected Areas). About 95% of the area –  
221 represented by 87% of the acquisitions – is covered by openly available GCA products. The  
222 total file size of GCA derived products is 3.2 TB.

223 Geographic coverage of the GCA extends to all biomes and biogeographic realms (Fig.  
224 1). The total number of acquisitions in the tropics is nearly twice as large (1,950) as in  
225 temperate regions (1,102) and six times as large as in the boreal zone (336). However,  
226 temperate and boreal acquisitions tend to cover larger areas and consequently the GCA  
227 comprises a total scan area of 20,271 km<sup>2</sup> (36% of the total) in the tropics, 27,543 km<sup>2</sup> in the  
228 temperate zone (49%, including Mediterranean forests), and 6,898 km<sup>2</sup> in boreal regions  
229 (12%). A few acquisitions (70) cover other biomes, such as mangroves or highly xeric systems  
230 with little woody canopy cover (1,842 km<sup>2</sup>, 3%).

231 In terms of bioclimatic space, the GCA spans a large gradient of mean annual  
232 temperatures, going from as low as -10 °C up to 30 °C, and ranges in precipitation from less  
233 than 100 mm a year to over 6,000 mm (Fig. 1b). The woody ecosystem structures sampled in  
234 the GCA are also highly diverse, from open systems with canopy cover of less than 10% and  
235 trees that never exceed 10-20 m, to dense, tall forests where canopy cover reaches close to  
236 100% and trees can exceed 100 m in height (Fig. 1c).



237

238 **Fig. 1: The Global Canopy Atlas.** The distribution of each of the 3,458 individual ALS acquisitions is shown (a)

239 on a map of the world, (b) in the environmental space, and (c) in terms of woody ecosystem structure. The top and

240 bottom rows show sample canopy height models (CHMs, 200×200 m) for 12 sample sites that span a wide variety

241 of ecosystems across the globe. Colours, ranging from dark blue to yellow with increasing height, are rescaled to  
242 fit the range of heights observed in each system, with the maximum height of the vegetation patch shown in the  
243 bottom right corner. The location of these 12 sites is also shown in geographic, environmental and structural space  
244 in panels (a–c) using numeric labels. Closed and open canopy ecosystem layers shown in (a) were derived by  
245 aggregating biomes in the Ecoregions2017 dataset (Dinerstein et al., 2017), for details cf. Table S3. Climatic  
246 variables in panel (b) were extracted from 1-km CHELSA climatologies for the years 1981-2010 (Karger et al.,  
247 2017) and averaged across the entire scan area. Maximum canopy height in panel (c) is defined as the 99<sup>th</sup>  
248 percentile of canopy height across the entire scan area. Canopy cover at 2 m is calculated as the percentage of  
249 CHM pixels  $\geq 2$  m.

250

251 In addition to the extensive sampling of geography, environment and woody ecosystem  
252 structure, the GCA covers large tracts of land that have been scanned more than once (Fig.  
253 S2). The area covered by repeated ALS acquisitions is 10,532 km<sup>2</sup> (19% of the total), but  
254 because several of these sites were scanned on multiple occasions the cumulative area of  
255 repeat acquisitions is 33,954 km<sup>2</sup>. This is more than 50% of the single-scan area coverage in  
256 the GCA, and brings the total scan area to 90,508 km<sup>2</sup>. Repeat acquisitions are available for  
257 all biomes, with the majority of the area covered by acquisitions on NEON sites in the United  
258 States of America (62%). The median interval between acquisitions is 1.2 years (95% range  
259 from 0.6 to 10.0 years).

260 In terms of sampling density and data quality, 93% of GCA acquisitions have an  
261 average pulse density  $>2$  m<sup>-2</sup>, and the median density across all acquisitions is 5.1 m<sup>-2</sup>. There  
262 is, however, a large spread around these values, with a 95% interval ranging from 1.2 to 123.1  
263 m<sup>-2</sup>. Temperate acquisitions in the GCA generally have higher pulse densities (median of 8.6  
264 m<sup>-2</sup>) than their tropical (4.9 m<sup>-2</sup>) or boreal (3.5 m<sup>-2</sup>) counterparts, and drone acquisitions have  
265 much higher densities (up to 1,000 m<sup>-2</sup>) than airplane and helicopter-based ones, but these  
266 high pulse density acquisitions only account for a small fraction of the database (49  
267 acquisitions  $> 300$  pulses m<sup>-2</sup>).

268 In terms of temporal coverage, acquisition dates range from 2006 to 2024, with 90%  
269 acquired between 2012 and 2022. More than 74% of acquisitions were completed within a 1-

270 week period (>94% within three months and >99% within six months). Most acquisitions have  
271 been acquired near or at peak EVI (87% of acquisitions) and NDVI (92%), with no clear  
272 geographic biases in acquisition timing. Uncertainty in ground classification is generally low.  
273 The average acquisition has topographic uncertainties over less than 2% of its area, and only  
274 51 acquisitions (~1.5%) have topographic uncertainties over more than 20% of the scanned  
275 area.

## 276 **4. Case studies**

277 All three case studies are based on analyses of CHMs generated using the locally adaptive  
278 spikefree algorithm (chm\_1spikefree.tif), as described in Tables 1 and S2. R code and ancillary  
279 data to replicate them are archived on Zenodo (<https://doi.org/10.5281/zenodo.16987211>).

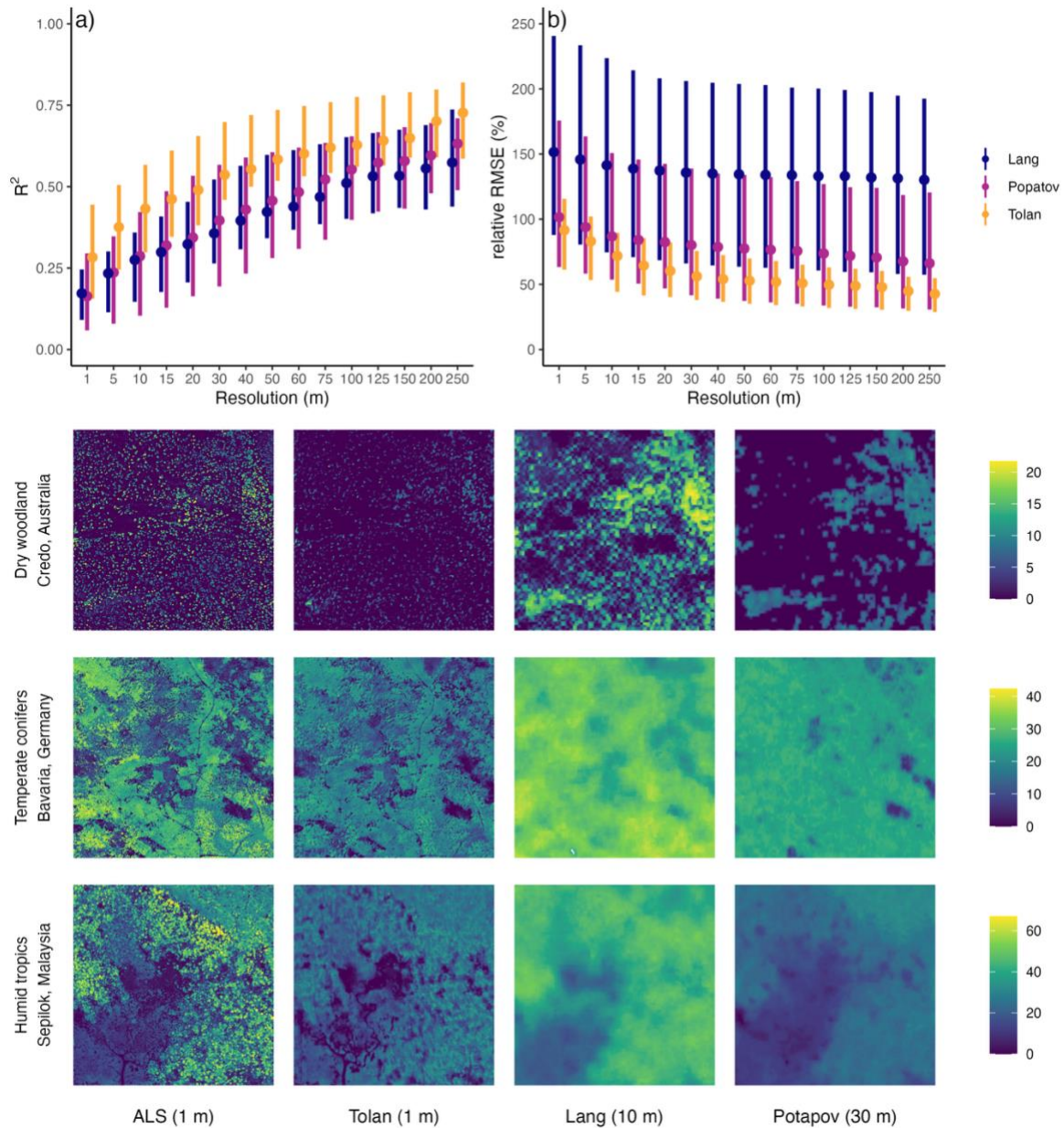
280

### 281 **4.1 Case study 1: How accurate are satellite-derived global canopy height models?**

282 Large-scale models of canopy height derived from satellite data are increasingly being used  
283 to map the structure and aboveground carbon storage of woody ecosystems (Liu et al., 2025;  
284 Schwartz et al., 2023; Wagner et al., 2025). At global scale, height maps are mostly created  
285 by combining wall-to-wall optical satellite imagery with laser scanning data acquired from  
286 space-borne or airborne sensors using machine learning. Three global examples include: (1)  
287 Potapov et al. (2021, 2022), who used Landsat imagery together with GEDI and ICESat-2  
288 shots to map canopy height at 30 m resolution, (2) Lang et al. (2023), who fused GEDI data  
289 and Sentinel-2 imagery to map canopy height at 10 m resolution; and (3) Tolan et al. (2024),  
290 who trained models on ALS data and predicted height from Maxar imagery at 1 m. However,  
291 while these models generally replicate global-scale gradients in canopy height, questions  
292 persist about their accuracy at landscape scale (Besic et al., 2025; Moudrý et al., 2024;  
293 Wagner et al., 2024). Optical satellite data have limitations both in open systems, where they  
294 underestimate tree cover (Brandt et al., 2020), and in closed canopy forests due to saturation  
295 effects (Mutanga et al., 2023). To address these concerns, we assessed the landscape scale  
296 accuracy of all three global canopy height models against ALS data from the GCA.

297 We compared the three satellite-derived height maps against ALS-derived CHMs from  
298 across 20 landscapes that had not been used to train the models. These ALS acquisitions  
299 span forest types with distinct 3D structures and were collected within 1-2 years of the satellite  
300 data used to generate the global models (Table S1.1). Agreement between ALS-derived  
301 products and the global maps was quantified by calculating the coefficient of determination  
302 ( $R^2$ ) and the relative root mean square error (RMSE), i.e., the RMSE standardized by the mean

303 canopy height. Since the global canopy height models differed in resolution, we first converted  
304 them to 1-m resolution via nearest-neighbour resampling and then calculated the  $R^2$  and  
305 RMSE across a wide range of resolutions between 1-250 m. By default, we averaged canopy  
306 height at each scale, but global models may represent different aspects of height (Besic et al.,  
307 2025), so we also calculated the  $R^2$  and RMSE for maximum height (99th percentile) at each  
308 resolution.



309

310 **Fig. 2. Accuracy of global canopy height models.** Panels (a-b) show the agreement between the three global  
311 canopy height models and ALS data across 20 landscapes at different spatial resolutions on the basis of  $R^2$  and

312 relative RMSE. Rasters are aggregated to different resolutions via averaging, with ALS data assumed to provide  
313 the true value. The distributions at each resolution are summarized via median values (dots) and 25<sup>th</sup> and 75<sup>th</sup>  
314 percentiles (error bars). Note that some data points exceeded 250% in relative RMSE, so have been excluded from  
315 the visualized range in panel (b). The panels below show sample canopy height models (2×2 km) from 3  
316 landscapes, including the reference ALS product at 1 m resolution. The height range of these maps is provided by  
317 the scale bars on the right. Examples of landscapes with particularly large errors for each of the three models can  
318 be found in Figs S1.4-1.6, an alternative assessment based on maximum canopy height in Fig. S1.1.

319         The three global canopy height models generally showed poor agreement with the  
320 reference ALS data (Fig. 2). At their nominal resolutions,  $R^2$  ranged from 0.28 (Lang, 10 m) to  
321 0.31 (Tolan, 1 m) to 0.38 (Potapov, 30 m). The corresponding errors were lowest for Tolan  
322 (relative RMSE = 95%), higher for Potapov (112%) and highest by some margin for Lang  
323 (189%). However, agreement depended strongly on resolution and tended to increase at  
324 coarser scales (Fig. 2a-b). When assessed at a common resolution of 30 m, the Tolan model  
325 clearly outperformed the other two models ( $R^2 = 0.54$  and RMSE = 58% compared to 0.38 and  
326 112% for Potapov, and 0.39 and 181% for Lang). The same was true at 250 m, where the  
327 Tolan model had an  $R^2$  of 0.65 and an RMSE of 43%, compared to the poorer 0.56 and 93%  
328 of Potapov and 0.56 and 170% of Lang. When comparing maximum heights instead of means,  
329 the differences in RMSE between models narrowed (57-69% at 30 m, 40-56% at 250 m; Fig.  
330 S1.1), but the accuracy of the predictions worsened ( $R^2 = 0.38-0.55$  at 250 m).

331         Global scale canopy height products are expected to be less accurate than costly high-  
332 resolution airborne laser scans, but our results highlight strong deficiencies in currently  
333 available global canopy height maps. While these products broadly mirror global height trends  
334 (Fig. S1.3), they miss most of the variation in canopy height within landscapes at their nominal  
335 resolutions (1–30 m). Even at 250 m resolution and for the best performing model (Tolan), the  
336 mean relative error was >40% of the reference height and reached as high as 170% in certain  
337 landscapes. This makes it near-impossible to capture within-landscape variation in canopy  
338 height with reasonable accuracy (Moudrý et al., 2024). We found that some models, such as  
339 the Lang model, predicted maximum canopy height better than mean height (Besic et al.,

340 2025), but errors still remained above 40%, and  $R^2$  values were even lower than for mean  
341 height. Across the vast majority of sites, the high-resolution approach of Tolan et al. (2024)  
342 was superior to other global maps tested here, with higher  $R^2$  and lower RMSE (Fig. 2), and  
343 better representation of landscape variability (Fig. S1.3). This may be due to an improved  
344 detection of trees from high-resolution imagery (Brandt et al., 2020) as well as the training on  
345 ALS data, which offer better resolution and geolocation than spaceborne lasers.

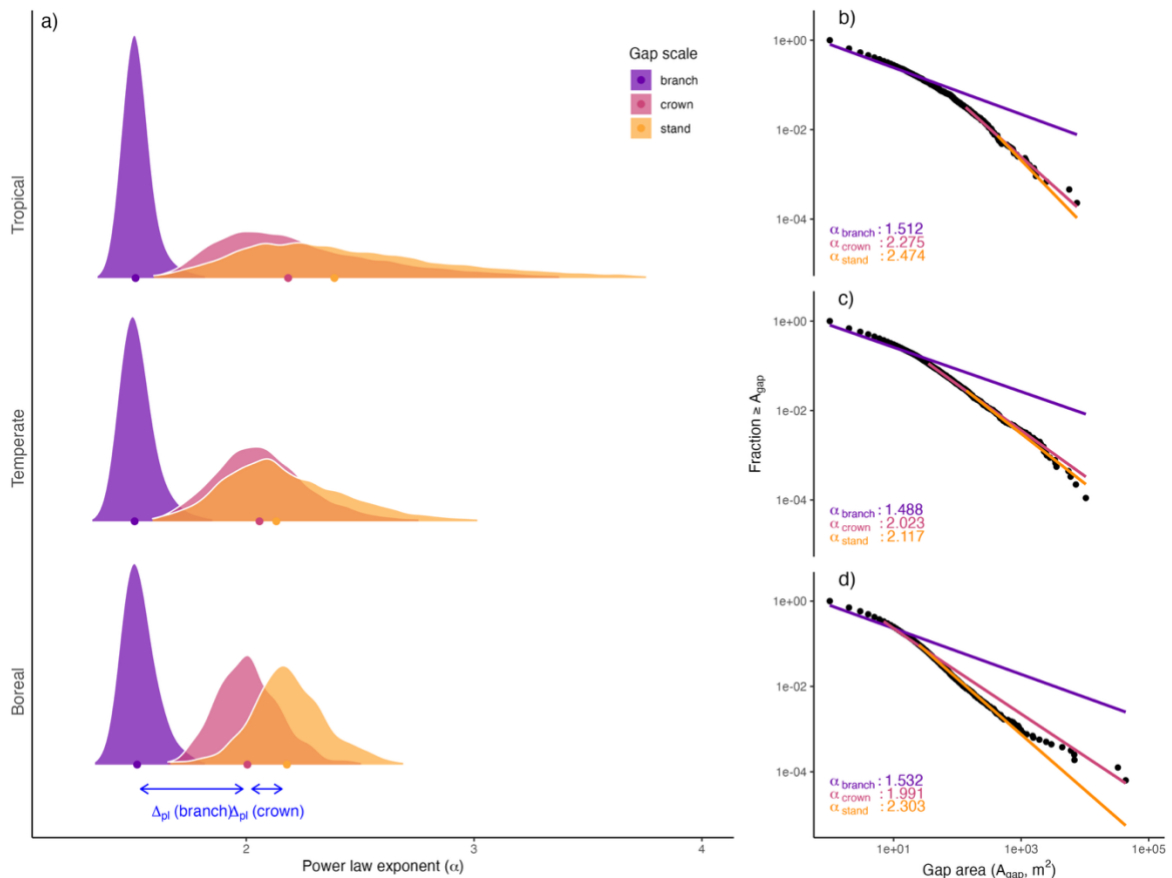
346         That being said, the Tolan height map also contained notable errors and uncertainties,  
347 underpredicting height at a tropical site in Amazonia by more than 20 m and consistently  
348 misrepresenting cloud cover as canopy gaps in tropical regions (Figs. S1.4-6). Global canopy  
349 height modelling is not even 15 years old (Simard et al., 2011) and we expect it to improve  
350 massively in the coming years, especially with the integration of new data sources (Quegan  
351 et al., 2019). It seems, however, that we are still a long way from operational products for  
352 global forest structure monitoring at medium to high resolution (1-30 m). Combining high-  
353 resolution satellite imagery with ALS for model training – as Tolan et al. (2024) have done –  
354 seems a promising approach. But it would require a more careful screening of input data (e.g.,  
355 removing cloud artefacts) and a wider range of ALS data for calibration. A recent canopy height  
356 model for Amazonia shows considerable potential in this respect (Wagner et al., 2025). We  
357 anticipate that the GCA, with its robust canopy height products available across all biomes,  
358 can serve as a benchmark for the calibration and validation of such models.

## 359 **4.2 Case study 2: Does the frequency of canopy gap sizes follow power laws?**

360 Treefall gaps are an essential component of forest structure and dynamics (Franklin et al.,  
361 1987). They reinitiate succession, create diverse forest microclimates and habitats (Ritter et  
362 al., 2005), and shape species composition (Denslow, 1987). As legacies of forest disturbance,  
363 they are key proxies for measuring canopy and carbon turnover (Dalagnol et al., 2021; Hunter  
364 et al., 2015; Jucker, 2022) and indices of how humans reshape ecosystem structure (Zhang  
365 et al., 2023). Over the last two decades, large-scale ALS surveys have revealed a fundamental  
366 pattern: small gaps are legion, and large gaps are rare. Regional-scale studies have often  
367 found that these heavy-tailed gap size frequency distributions (GSFD) exhibit power law  
368 scaling (Goodbody et al., 2020; Kellner & Asner, 2009), possibly with a narrow range of  
369 exponents (Asner et al., 2013). If true at global scale, this would imply an astonishing level of  
370 generalization: (1) that forest dynamics are governed by multiplicative processes, (2) that  
371 these processes show little variation from the boreal to the tropics and (3) that they are scale-  
372 invariant, i.e., small-scale disturbances such as branchfalls follow similar rules as large-scale  
373 disturbances such as those associated with wildfires and storms. However, not all studies  
374 show power law scaling (Araujo et al., 2021), and scale invariance has never been  
375 systematically tested at global scales. Comparisons between regional studies are complicated  
376 if not impossible, as the inferred exponents depend on how CHMs are derived (Fischer et al.,  
377 2024; White et al., 2018), how gaps are defined (Asner et al., 2013; Lobo & Dalling, 2014),  
378 and how power laws are fitted (Hanel et al., 2017; Wedeux & Coomes, 2015). Since power  
379 laws are difficult to distinguish from other heavy-tailed distributions (Newman, 2005; Taubert  
380 et al., 2013), it is an open question whether GSFDs follow power laws across forest types,  
381 spatial scales, and the range of gap sizes.

382 To systematically tackle this question, we chose a subset of high-quality CHMs from  
383 the GCA with a minimum of 70% canopy cover at 2 m and divided them into 1 km<sup>2</sup> cells using  
384 a flexible Voronoi tessellation (n = 13,300, details on selection in Supplementary S2.1). For  
385 each 1 km<sup>2</sup> cell we calculated the mean canopy height ( $\mu_{\text{CHM}}$ ) and defined gaps as contiguous

386 areas (rook neighborhood) below a height threshold of  $\delta_{\text{CHM}} = 0.5 \times \mu_{\text{CHM}}$  and no larger than  
387 100,000 m<sup>2</sup> (10% of the reference area). This excluded some larger gaps, but was not  
388 expected to alter power law assessments below 100,000 m<sup>2</sup>. Gap size was calculated as the  
389 number of 1 m<sup>2</sup> pixels in a gap (Kellner & Asner, 2009), and discrete power laws were fitted  
390 with the `powerlaw` R package (Gillespie, 2015). Tests for power law behaviour exist, but  
391 reduce a continuous spectrum of deviations to binary hypothesis testing and are difficult to  
392 interpret (Hanel et al., 2017). We therefore used an alternative heuristic that quantifies  
393 deviations from scale invariance (Fischer & Jucker, 2024). Under ideal power law behaviour,  
394 the scaling exponent  $\alpha$  is scale-invariant. If a power law is fit to the full range of gap sizes and  
395 to a subset (e.g., only large gaps),  $\alpha$  should be approximately identical. If  $\alpha$  differs, we can  
396 calculate a deviation from power-law scaling  $\Delta_{\text{PL}}$  as the difference between both  $\alpha$  values. We  
397 here calculated  $\Delta_{\text{PL}}$  over three different scale ranges. First, we calculated  $\alpha$  for all gaps from  
398 small branch falls  $\geq 1$  m<sup>2</sup> up to 100,000 m<sup>2</sup> ( $\alpha_{\text{branch}}$ ). This is the lower cutoff used in Kellner &  
399 Asner (2009). The mean area of all gaps within that range was 32.8 m<sup>2</sup> (95% range: 9.4 to  
400 91.8 m<sup>2</sup>). Second, we calculated  $\alpha$  only for single treefall gaps or larger ( $\alpha_{\text{crown}}$ ). Crown area  
401 scales with tree height (Jucker et al., 2022), so we approximated the typical tree crown area  
402 as circle with a diameter equivalent to the height cutoff  $\delta_{\text{CHM}}$  in each 1 km<sup>2</sup> cell ( $0.25 \times \delta_{\text{CHM}}^2 \times$   
403  $\pi$ ). The corresponding mean gap area was 420.4 m<sup>2</sup> (60.3 to 1,446.7 m<sup>2</sup>). Finally, we  
404 calculated  $\alpha$  only for the tail end of the gap size frequency distribution ( $\alpha_{\text{stand}}$ ). For this, we  
405 calculated the cutoff as the midpoint between the typical tree crown size and the size of the  
406 largest disturbances (95<sup>th</sup> percentile of gap sizes). The mean gap area was 1,830.9 m<sup>2</sup> (210.0  
407 to 5691.1 m<sup>2</sup>). Deviations were then quantified as  $\Delta_{\text{PL, branch}} = \alpha_{\text{crown}} - \alpha_{\text{branch}}$  and  $\Delta_{\text{PL, crown}} = \alpha_{\text{stand}}$   
408  $- \alpha_{\text{crown}}$  and calculated separately for boreal forests (n = 501), temperate forests (n = 3,903)  
409 and tropical forests (n = 8,896). The robustness of results was tested through several  
410 sensitivity analyses (Figs. S2.2-2.7).



411

412 **Fig. 3: Deviations from power law scaling across major biomes.** Panel (a) shows the distribution

413 of power law exponents of gap size frequency distributions ( $\alpha$ ) for 1 km<sup>2</sup> cells across tropical, temperate

414 and boreal biomes and coloured by the size ranges over which they are calculated ( $\alpha_{crown}$ ,  $\alpha_{branch}$  and

415  $\alpha_{stand}$ ). Coloured points represent the median values of the distributions. Under true power law

416 behaviour,  $\alpha$  should not depend on the size range over which it is calculated, so all distributions should

417 be indistinguishable, with a near-identical median or mean ( $\Delta_{PL} \approx 0$ ). The righthand column (b–d) shows

418 results from a sample 1 km<sup>2</sup> cell in each of the three biomes to illustrate how  $\alpha$  varies across scales.

419 Each black point represents the contribution of a single gap to the the observed complementary

420 cumulative distribution function (CCDF) of gap sizes, plotted on double-logarithmic scales. Coloured

421 lines show the fitted power laws. We chose a CCDF representation over size frequency plots, as it

422 avoids binning into size classes and noise in the tail end (Newman, 2005). Sample data are from a

423 tropical site in Indonesian Borneo (b), a temperate site in Northwestern United States (c), and a boreal

424 site in Québec, Canada (d) and were selected to be close to each biome's median in  $\alpha_{branch}$  and  $\alpha_{crown}$ .

425

426 We found that the power law exponent  $\alpha$  was highly scale dependent, indicating that GSFDs

427 do not follow power law behaviour (Fig. 3). When small gaps were included,  $\alpha$  was low and

428 narrowly distributed within and across biomes (mean  $\alpha_{branch} = 1.52$ ; 95% interval = 1.42-1.70).

429 By contrast, when focussing on gaps from treefalls or larger disturbances, exponents were

430 considerably higher and much more variable ( $\alpha_{\text{crown}} = 2.22$ ; 1.73-3.28), even though the gaps  
431 excluded in the  $\alpha_{\text{crown}}$  calculation only made up 2.59% (0.74-5.21) of the total gap area. Across  
432 biomes, tropical forests generally had the largest  $\alpha_{\text{crown}}$  and the largest variation around the  
433 mean (2.29; 1.73-3.45), compared to boreal (2.02; 1.76-2.38) and temperate forests (2.08;  
434 1.71-2.61). From branch to crown scale, the typical deviation from power law scaling  $\Delta_{\text{PL, branch}}$   
435 was 0.70 (0.16-1.73) and was highest in the tropics (0.77) and smallest in boreal landscapes  
436 (0.49). Exponents increased again, albeit much less, when excluding treefall gaps and only  
437 fitting power laws to the largest disturbances ( $\alpha_{\text{stand}} = 2.38$ ; 1.73-3.63 and  $\Delta_{\text{PL, crown}} = 0.25$ ; -  
438 0.23-0.91). Qualitatively, our results were robust to methodological choices, with  $\alpha$  changing  
439 across scales and biomes also for different CHM types (Figs. S2.2–2.5) and when applying  
440 fixed thresholds to define gaps ( $< 2$  m) and minimum gap size ( $\geq 9$  m<sup>2</sup>, Figs. S2.6–2.7).

441 Overall, our results provide strong evidence that GSFDs do not follow power laws. The  
442 violation of scaling behaviour points to fundamentally different processes shaping forest  
443 structure at small and at large scales (Shugart et al., 2010). When GSFDs include small,  
444 branch-level gaps, inferred power law coefficients tend to be small and highly consistent  
445 across systems (Fig. 3), but at larger scales they exhibit tremendous variability that reflects  
446 the “fingerprints” of different disturbance regimes (Jucker, 2022). Violations of fundamental  
447 scaling assumptions likely explain why previous studies have come to different conclusions  
448 about the typical values and variability of power law coefficients (Asner et al., 2013; Goodbody  
449 et al., 2020; Reis et al., 2022), with differences exacerbated by CHM construction (Fig. 3 vs.  
450 Fig. S2.2, White et al., 2018). Based on our results ( $\Delta_{\text{PL, crown}} \ll \Delta_{\text{PL, branch}}$ ) and in line with  
451 observations in other systems (Newman, 2005), it is possible that GSFDs converge to power  
452 law behaviour at the tail end of the distribution, but our case study reveals a fundamental scale  
453 dependence across a large size range. A wider range of functions to model GSFDs (Araujo et  
454 al., 2021), combined with collections such as the GCA, will help build a more comprehensive  
455 picture of global forest structure and how it is shaped by natural and anthropogenic  
456 disturbances.

457

### 458 **4.3 Case study 3: How dynamic are forest canopies?**

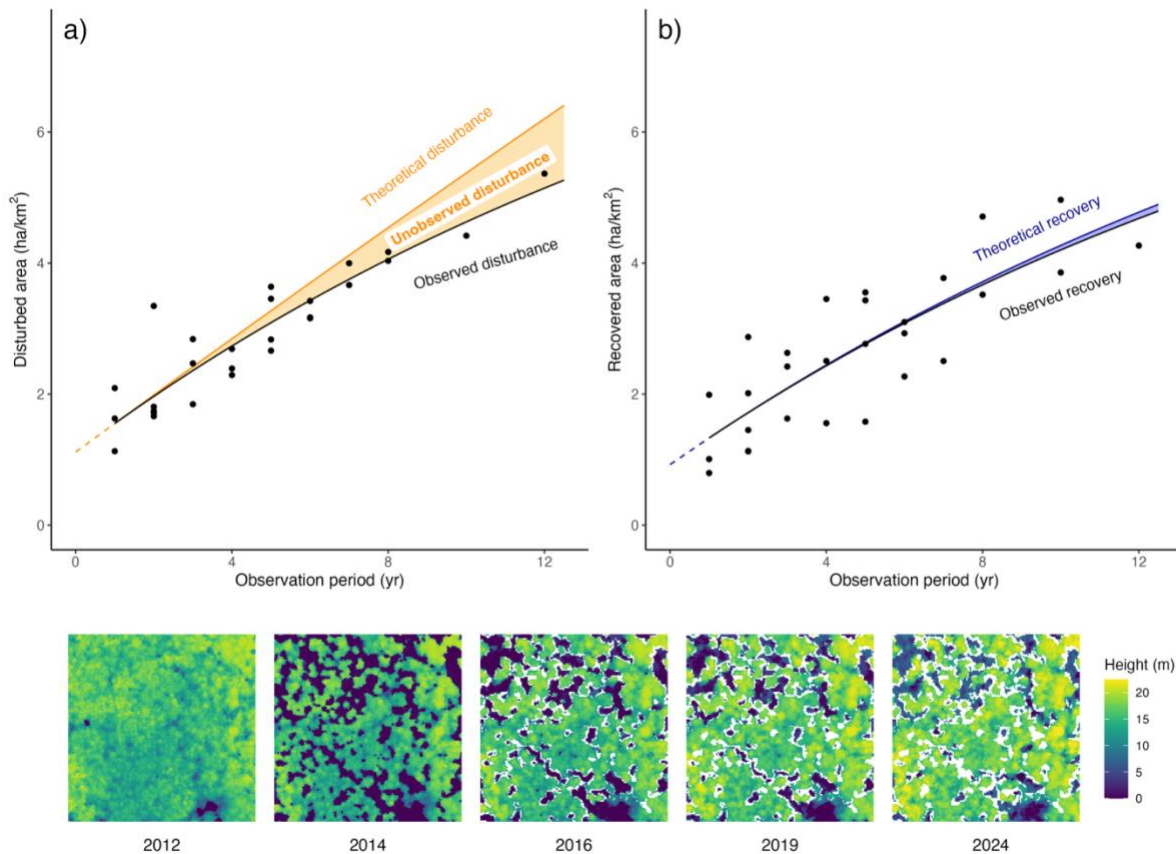
459 Accurate monitoring of forest growth and disturbance through time is an essential first step in  
460 understanding drivers of forest dynamics and forest responses to global change. Collections  
461 such as the GCA bring together ALS data from many sources and years. Many of these  
462 acquisitions overlap spatially, which creates the opportunity for large-scale repeat surveying  
463 of forests, in particular the monitoring of growth (Yu et al., 2004), disturbance (Huertas et al.,  
464 2022), recovery (Krüger et al., 2024), biomass change (Cao et al., 2016; Næsset et al., 2013),  
465 structural complexity (Rosen et al., 2024), and tree demographics (Battison et al., 2024).  
466 However, estimating change rates from multi-temporal and multi-source ALS comes with its  
467 own set of challenges and depends on instrument differences and methodological decisions  
468 (Jackson et al., 2024; Leitold et al., 2018). When intervals between acquisitions are short (1-  
469 5 years), small biological changes are easily confused with measurement errors (Heiskanen  
470 et al., 2024; Riofrío et al., 2022). By contrast, as intervals between acquisitions get longer,  
471 disturbances can be missed or underestimated in size due to rapid recovery between  
472 acquisitions or repeat disturbances in the same area. These transient disturbances and  
473 recovery events parallel the problems of unobserved tree mortality and growth in field  
474 inventories with long remeasurement intervals (Kohyama et al., 2019), but have not been  
475 explored for repeat ALS surveys. We here leverage a unique timeseries of 8 ALS acquisitions  
476 conducted over a period of 12 years at Harvard Forest in the Northeastern United States and  
477 propose a new approach to robustly estimate disturbance and recovery rates, instrumentation  
478 noise, and transient dynamics.

479 Harvard Forest is part of the National Ecological Observatory Network (NEON). It is a  
480 mixed temperate forest dominated by deciduous broadleaf trees (*Quercus rubra*, *Acer rubrum*)  
481 and white pine (*Pinus strobus*), with a mean canopy height of ~17 m and canopy cover of  
482 ~80%. The GCA contains 12 ALS acquisitions for Harvard Forest, but for the purposes of this  
483 analysis we focussed on 8 summer acquisitions conducted by NEON (2012, 2014, 2016, 2017,  
484 2018, 2019, 2022, and 2024), as these cover a large area of overlap (~145 km<sup>2</sup>, all pulse  
485 densities > 2 pulses m<sup>-2</sup>). Each acquisition's CHM was split into tiles of 1 km<sup>2</sup>. For each cell,

486 we defined gaps as contiguous areas (rook neighborhood) below 10 m canopy height. Non-  
487 forest areas were defined as those lower than 10 m in canopy height which changed by less  
488 than 2 m over 12 years, and masked out. We calculated dynamics between each pair of NEON  
489 acquisitions (28 combinations), differentiating disturbance (newly formed gap area as  
490 proportion of intact canopy area), and recovery (closed gap area as a proportion of previous  
491 gap area; Jackson et al., 2024). Assuming a typical yearly disturbance rate  $d$  and recovery  
492 rate  $r$ , expressed as proportion of initial canopy and gap area, we derived an analytic  
493 relationship between those rates and the observed disturbance and recovery for a given time  
494 interval between surveys (Supplementary Material S3.1). This allowed us to separate  
495 between-scan noise ( $d_0$  and  $r_0$  for disturbance and recovery) from biological signal and to  
496 estimate unobserved dynamics by comparing observed rates to the theoretical rates that  
497 would apply if there were no transient events (no short-term recovery after gap formation, no  
498 immediate re-disturbance after closure). We fitted the models via the *brms* R package  
499 (Bürkner, 2018, Supplementary Material S3.2) and explored the sensitivity of results to  
500 modelling decisions (Supplementary Material S3.3-3.4).

501 We found near steady-state dynamics at Harvard Forest, with disturbance slightly  
502 exceeding recovery (Fig. 4). We estimated a 1-year gap creation rate of  $d = 0.45 \text{ ha km}^{-2}$  (95%  
503 interval = 0.36-0.64) or slightly less than 0.5% of the intact canopy area ( $\sim 90 \text{ ha km}^{-2}$ ), and a  
504 1-year gap recovery rate  $r = 0.41 \text{ ha km}^{-2}$  (0.07-1.11), or slightly less than 5% of the disturbed  
505 area ( $\sim 10 \text{ ha km}^{-2}$ ). After accounting for biases due to between-scan noise ( $d_0 = 1.09 \text{ ha km}^{-2}$ ,  
506  $0.64\text{-}1.54$ , and  $r_0 = 0.93 \text{ ha km}^{-2}$ ,  $0.68\text{-}1.17$ ), we inferred a total of  $5.30 \text{ ha km}^{-2}$  (4.26-7.34)  
507 of newly created gaps and  $3.86 \text{ ha km}^{-2}$  (0.85-7.26) of recovered canopy area over 12 years.  
508 Of the new gaps, an estimated  $1.11 \text{ ha km}^{-2}$  ( $\sim 21\%$ ) had closed again by 2024, and  $0.1 \text{ ha km}^{-2}$   
509 ( $\sim 3\%$ ) of closed gaps had re-opened after closure. In canopies with higher turnover, we  
510 estimated that such transient dynamics could account for up to 57% (short-term recovery of  
511 gaps) and 7% (re-disturbance of recovered area), respectively ( $d = r = 2.0 \text{ ha km}^{-2}$ , Fig. S3.1).  
512 Our estimates varied slightly, but not fundamentally, when introducing a minimum gap size ( $d$   
513  $= 0.45 \text{ ha km}^{-2}$ ,  $r = 0.34 \text{ ha km}^{-2}$ , Fig. S3.2) or subsetting to a smaller area where additional

514 acquisitions were available ( $d = 0.58 \text{ ha km}^{-2}$ ,  $r = 0.38 \text{ ha km}^{-2}$ , Fig. S3.3). Inferences from  
515 single pairs of acquisitions were more uncertain ( $d \sim 0.24\text{-}1.11 \text{ ha km}^{-2}$  and  $r \sim 0.05\text{-}1.04 \text{ ha}$   
516  $\text{km}^{-2}$ ), but the overall averages were consistent ( $d = 0.45 \text{ ha km}^{-2}$ ,  $r = 0.40 \text{ ha km}^{-2}$ , Fig. S3.4).  
517 Estimates of biases due to between-scan noise were confirmed independently via temporally  
518 coincident acquisitions ( $d_0 = 0.89 \text{ ha km}^{-2}$ ,  $0.19\text{-}3.19$ ,  $r_0 = 0.94 \text{ ha km}^{-2}$ ,  $0.28\text{-}2.82$ , Fig. S3.5).



519  
520 **Fig. 4. Short-term dynamics at Harvard Forest.** Panels show observed rates of (a) disturbance  $d$  and (b) recovery  
521  $r$  as a function of the time interval (years) between successive ALS surveys (black points). As the intervals between  
522 observations get longer (a), an increasing proportion of disturbances recover before being re-surveyed, leading to  
523 an underestimation of true disturbance rates (and equivalently for recovery in panel b). Rates were inferred as  
524 proportion of existing canopy and gap area and then converted into area rates per grid cell ( $\text{ha km}^{-2}$ ). Black lines  
525 are fitted relationships, while coloured lines reflect the theoretical changes that would be expected if there was no  
526 short-term recovery of disturbed area (a) and no rapid re-disturbance of recovered area (b). They are calculated  
527 by extending  $d$  and  $r$  into the future, discounting only for loss of canopy and gap area, respectively. The intercepts  
528  $d_0$  and  $r_0$  are non-zero, as a proportion of pixels is expected to switch randomly between gap and non-gap states  
529 between two ALS acquisitions (e.g., due to instrument differences or movement of leaves) and thus introduce a  
530 baseline bias in disturbance and recovery rates. The five panels below show a sample canopy height model at

531 Harvard Forest (150×150 m) over a 12-year period. White contours indicate gaps or parts of gaps that formed  
532 between 2012 and 2014 and rapidly closed in the years afterwards. These would go undetected in a direct  
533 comparison between 2012 and 2024. The panels show that initial gap recovery stems predominantly from lateral  
534 ingrowth around gaps, and within-gap regeneration appears only in 2024 as lighter blue areas within gaps.

535 Our results show a moderately dynamic canopy at Harvard Forest, with close to 1% of the  
536 area (1 ha km<sup>-2</sup>) either disturbed or recovering year-to-year, and more than 20% of the gap  
537 area created by branch or treefalls closing again over 12 years (Fig. 4, bottom panels). This  
538 transient turnover, which we cannot observe when ALS acquisitions are repeated infrequently,  
539 is expected to be even larger in forest canopies with higher disturbance and recovery rates  
540 (Fig. S3.1). To quantify it, we need medium-to-high frequency monitoring programs (e.g.,  
541 Cushman et al., 2022) and robust methods that can account for scanning noise. We found  
542 that nearly 2% of the pixels were expected to switch from canopy to gap status (~1%) or vice  
543 versa (~1%) simply due to measurement noise between ALS acquisitions. This was more than  
544 twice the mean yearly biological changes at Harvard Forest, and if not accounted for, would  
545 greatly inflate estimates of canopy dynamics. Single pairs of acquisitions may be particularly  
546 affected by these issues (Heiskanen et al., 2024), which can be further compounded by  
547 ecological variability, changes in acquisition timing (cf. “winter” outliers in Fig. S3.3a) or  
548 instable CHM algorithms (Fischer et al., 2024). Some instrumentation noise may be avoided  
549 by careful re-calibration (Riofrío et al., 2022) or by subsetting to larger or more severe  
550 disturbances (Fig. S3.2). However, the former is challenging, and the latter does not make  
551 biological sense when tracking recovery which is more gradual in nature (Körner, 2003). A  
552 more robust approach will consist in the pooling of information across multiple sites and  
553 acquisitions per site, ideally via Bayesian hierarchical models (Kohyama et al., 2018). Long-  
554 term ecological observatories such as NEON and harmonised collections like the GCA will  
555 provide an ideal backbone for such an approach and enable us to sketch a global picture of  
556 canopy turnover.

## 557 **5. Outlook**

### 558 **5.1 In Humboldt's and Bonpland's tailwinds**

559 Ever since Alexander von Humboldt and Aimé Bonpland set out to travel the Americas,  
560 comparing ecosystems and communities across large geographic gradients has been a  
561 cornerstone of modern Earth system science. On the one hand, ecosystems display a large  
562 degree of local idiosyncrasy, shaped as much by their unique geological and climatic past as  
563 the accidents of natural and human history. On the other hand, there are commonalities in  
564 how ecosystems develop that cut across biomes, continents and civilizations. These are  
565 encoded in vegetation structural patterns, such as how height and cover depend on water  
566 availability (Staver et al., 2011; Tao et al., 2016), how growing season length limits the  
567 elevation range of trees (Paulsen & Körner, 2014), and the successional mosaics left behind  
568 by natural and anthropogenic disturbance (Frelich et al., 2018; Jucker, 2022). Describing these  
569 patterns, identifying new ones, and linking them to the biophysical processes that underpin  
570 them not only enhances our understanding of the natural world, but also improves our ability  
571 to predict ecosystem responses to global change in decades to come (Blois et al., 2013).  
572 Remote sensing technologies such as ALS are uniquely poised to carry this project forward  
573 (Senf, 2022). Much of global ecology so far has been informed by a combination of local field  
574 samples and optical satellite layers – providing a “flat” view of the world as a tapestry of  
575 landcovers, punctuated by occasional data-rich information spikes grounded in field  
576 observations. ALS inserts 3D contours into this 2D world, converting discrete vegetation  
577 classes (e.g., forest and non-forest) into continuous vegetation metrics (e.g., vegetation  
578 height, cover and density). In doing so it helps us build a fuller and more nuanced picture of  
579 woody ecosystem structure and how it reflects current as well as past dynamics (Lenoir et al.,  
580 2022).

581 As we showed here, ALS can be a particularly powerful macroecological tool when  
582 acquisitions from different sources, sites and times are harmonized in large databases such  
583 as the GCA. High-resolution derived products such as CHMs and DTMs are comparatively

584 small in size, robust, and easily analysed and interpreted with a wide range of software  
585 (Fischer et al., 2024). These detailed but accessible ecosystem maps shift the focus from  
586 resource-intensive data processing to ecological analysis, model building and technological  
587 innovation (White et al., 2019). As highlighted by our case studies, it requires comparatively  
588 little effort to use 3D maps to validate predictions from satellite-based sensors (case study 1).  
589 carry out robust global comparisons of complex structural features (case study 2) and  
590 precisely quantify ecosystem dynamics through time (case study 3). Naturally, our case  
591 studies offer only a glimpse into the opportunities provided by regional to global ALS  
592 harmonization. Comparisons of ALS-derived maps across and within biomes may  
593 fundamentally shift our conceptualization of ecosystem dynamics (Lines et al., 2022) and  
594 usher in a new generation of ecosystem models (Shugart et al., 2015). Future versions of the  
595 GCA and other similar projects could provide harmonised ALS collections covering even larger  
596 spatial extents, such as wall-to-wall maps of entire countries or continents (Moudrý et al.,  
597 2024). They could also be used to derive additional information from point clouds that goes  
598 beyond rasterized maps of height, such as leaf area densities (Vincent et al., 2023) and  
599 subcanopy structure (Jarron et al., 2020), further enhancing our picture of the 3D structure of  
600 the world's terrestrial ecosystems.

## 601 **5.2 Flying close to the ground**

602 The new picture of woody ecosystem structure will take time to develop. When Humboldt and  
603 Bonpland arrived in Venezuela, they were so enthralled by the flora and fauna that they ran  
604 from one organism to the next like “madmen” (Humboldt, 1801). It then took them decades to  
605 systematize their knowledge. The characterisation of ecosystem structure from remote  
606 sensing and ALS is likely in a similar situation. Laser scanning has come a long way since its  
607 first applications in forestry, which date back to the 1970s and 1980s (Nelson, 2013). We now  
608 possess vast amounts of data and a wide range of tools to analyse them (Coops et al., 2021;  
609 Næsset, 2002; Roussel et al., 2020), but, in our characterization of global ecosystems, we are  
610 likely still in the initial exploration phase and will require years of consolidation to arrive at

611 robust categorizations and predictions (Atkins et al., 2018; Fassnacht et al., 2024; Knapp et  
612 al., 2020; Loke & Chisholm, 2022; Rosen et al., 2024; Valbuena et al., 2020). The GCA  
613 provides a strong foundation for this enterprise. Its ecosystem maps provide samples from a  
614 wide range of environments (Wulder, White, Nelson, et al., 2012), have been developed to be  
615 maximally robust to differences between acquisitions (Fischer et al., 2024), and are  
616 accompanied by extensive metadata, quality layers and masks that can be used to identify  
617 areas where robustness may be compromised (Table S2).

618 Automated data processing and quality checks have their limitations, and for certain  
619 applications (e.g., measurements of within-canopy structure) additional corrections or data  
620 filtering may be needed, including targeted ground corrections (Riofrío et al., 2022), manual  
621 re-classification, or adjustments to account for instrument properties (Roussel et al., 2017;  
622 Vincent et al., 2023). Furthermore, as our case studies show, the need for careful analysis  
623 goes beyond these initial data selection and processing steps and extends to ecological model  
624 building itself. Just because we can predict canopy height from ALS-trained satellite data (case  
625 study 1), fit power laws to gap sizes (case study 2) or calculate structural change between  
626 successive acquisitions (case study 3) does not mean the results are always reliable or useful.  
627 Robust global ecosystem ecology needs to be guided by a biophysical understanding of the  
628 underlying dynamics, a careful selection of metrics to monitor them (Fischer et al., 2024;  
629 Zhang et al., 2024), models that can account and correct for biases, and standardized  
630 methods to assess their predictive power and transferability (Ploton et al., 2020; Tompalski et  
631 al., 2019). A key challenge going forward is to link ALS observations back to field data and  
632 fundamental ecological units such as trees and species (White et al., 2016). This will be  
633 facilitated by a wide range of methods, such as manual and automatic tree segmentation  
634 (Aubry-Kientz et al., 2021; Weinstein et al., 2021), model inversion (Shugart et al., 2015), or  
635 algorithms that attempt to reconstruct inventories bottom-up (Fischer et al., 2020; Spriggs et  
636 al., 2015; Taubert et al., 2015)

### 637 **5.3 Flying together**

638 Science is a social enterprise, and global databases such as the GCA are community efforts  
639 made possible by the collective investments, work and ideas of researchers across nations,  
640 generations and disciplines. While this creates a unique opportunity for collaborative research  
641 and data sharing, it also brings a responsibility to promote fair use. Access to and utilization  
642 of data are shaped by country-specific procurement models and regulatory openness as well  
643 as historical power asymmetries, such as those that often divide the Global South and Global  
644 North (de Angeli Dutra et al., 2025) or countries in and outside the tropics (de Lima et al.,  
645 2022). Such asymmetries are a particular concern with regard to remote sensing technologies  
646 such as ALS, which rely on expensive instruments and can be employed by domestic or  
647 foreign actors without meaningful involvement of local communities or researchers. The open  
648 release of such data is key as it creates opportunities for local experts and a wider public to  
649 actively contribute to research. Equally important are clear licensing and documentation that  
650 acknowledge local data contributors and institutions, ongoing support for acquisitions in  
651 undersampled areas and investments in capacity building. Care is also required to avoid  
652 misuse of data. Easily accessible remote sensing data could be used for the surveillance of  
653 communities (Millner et al., 2024) or to reveal the location of environmental assets (e.g.  
654 logging and mining opportunities) and archaeological sites (Fisher et al., 2021), potentially  
655 exacerbating disparities where access and safeguards are uneven. Moreover, external actors  
656 may violate data-ownership laws or license terms (e.g. non-commercial clauses), or  
657 repackage publicly available data into commercial products without proper attribution.

658 The GCA project cannot solve these problems by itself, but it can take steps to mitigate  
659 risks. First, by provisioning standardized ALS-derived products, but not the raw data, the GCA  
660 provides added value, but does not supplant the original data sources, which are thoroughly  
661 documented and linked to (cf. Table S1). Second, with its focus on simple, light-weight raster  
662 products, the GCA reduces the need for expensive computing infrastructure to process and  
663 analyse data. Third, it brings visibility to acquisitions missing from large open data repositories,

664 which we hope will increase collaboration opportunities for local experts. Finally, the GCA has  
665 a relatively equal distribution of data in space, with representative coverage across the tropics  
666 (Fig. 1), ensuring that new products – often trained and tested in high-latitude temperate and  
667 boreal zones – become more representative of ecosystems and research needs globally. On  
668 balance, we believe that the benefits of making the majority of the GCA's products openly  
669 available outweigh the risks. Most raw data in the GCA are already open, so the publication  
670 of harmonised, easy-to-use derived products should mostly benefit local researchers and  
671 practitioners who do not have the means to find, store and process large volumes of raw data.  
672 Past experience has shown that pre-processed openly available global datasets, such as  
673 meteorological and climate layers (Fick & Hijmans, 2017) and global trait compilations (Zanne  
674 et al., 2009), can greatly benefit researchers world-wide and fill gaps in areas where  
675 specialized local products and data are not as readily accessible.

676 To ensure the GCA promotes scientific discovery in a fair and equitable manner, we  
677 aim to implement a number of measures to further widen participation in the maintenance and  
678 governance of the database. This includes appointing an advisory committee to guide how  
679 best to continue growing the GCA in a way that does not unintentionally reinforce historical  
680 power imbalances. Similarly, we aim to invite local experts to join the project to help assemble  
681 ancillary datasets for the GCA landscapes so that we can build a richer picture of their ecology  
682 and history. Further, we plan to organise targeted online and in-person training courses  
683 designed to lower the barrier to entry for working with ALS data and facilitate their integration  
684 into existing research programs underway across GCA landscapes. Above all, we hope that  
685 we can encourage users of the database, particularly in the Global North, to contribute to these  
686 goals by involving local experts in their studies and investing in the maintenance and growth  
687 of the GCA network.

688

## 689 **Acknowledgements**

690 Databases such as the GCA would not be possible without the work and investments of  
691 countless scientific and non-scientific actors that support data collection efforts in the field as

692 well as the checking, analysis, and maintainance of data. We deeply thank all of them for their  
693 dedication and support.

694

695 FJ Fischer and T Jucker acknowledge a Research Project Grant from the Leverhulme Trust  
696 to T Jucker (grant: RPG-2020-341). FJ Fischer and R Seidl acknowledge the European  
697 Research Council under the European Union’s Horizon 2020 research and innovation program  
698 (Grant Agreement 101001905, FORWARD). T Jucker acknowledges a UK NERC  
699 Independent Research Fellowship (grant: NE/S01537X/1) and UKRI Frontier Research grant  
700 (grant: EP/Y003810/1). J Chave and N Labrière acknowledge ESA FRM4BIOMASS and  
701 Labex CEBA (ANR-10-LABX-25-01). KC Cushman and M Krassovski were supported by the  
702 Laboratory Directed Research and Development Program of Oak Ridge National Laboratory  
703 (ORNL); ORNL is managed by the University of Tennessee-Battelle, LLC, under contract DE-  
704 AC05-00OR22725 with the U.S. Department of Energy. K Stereńczak acknowledges Project  
705 LIFE+ ForBioSensing (contract number LIFE13ENV/PL/000048) and Poland’s National Fund  
706 for Environmental Protection and Water Management (contract number  
707 485/2014/WN10/OPNMLF/D) and project “AFTER FBS – maintenance of ForBioSensing  
708 project performance indicators,” which is funded by the Forest Research Institute’s own  
709 research fund (no. 261509). J Aguirre-Gutiérrez acknowledges the Natural Environment  
710 Research Council (NERC; NE/T011084/1 and NE/Z504191/1), the Leverhulme Trust (RPG-  
711 2024-342) and the Royal Society (RG/R1/251370). A Burt and M Demol acknowledge support  
712 for data acquisitions in Gilé NP from a. World Bank through the Forest Carbon Partnership  
713 Facility b. Government of Mozambique through the Monitoring, Reporting and Verification Unit  
714 of the National Fund for Sustainable Development and c. Innovate UK (project number  
715 10004871). J Cervenka acknowledges support from cross-border cooperation programme  
716 Czech Republic–Bavaria Free State ETC goal 2014–2020, the Interreg V project No. 99. F  
717 Fassnacht, J Schäfer, H Weiser and B Höfle acknowledge Deutsche Forschungsgemeinschaft  
718 (DFG, German Research Foundation) Project SYSSIFOSS - 411263134/2019-2022. L  
719 Fatoyinbo was supported by NASA Land Cover Land Use Change and Carbon Monitoring

720 System Program. Eric Bastos Görgens was supported by CNPq grants 403297/2016-8,  
721 401053/2019-9, 306386-2022-4. Amazon Fund grant 14.2.0929.1. USAID AID-OAA-A-11–  
722 00012. Acquisitions of airborne LiDAR data, contributed by T Gorum, were funded by DELTA  
723 Lidar, Türkiye. H Guan acknowledges the National Natural Science Foundation of China  
724 (32401574). Acquisition of airborne LiDAR data acquisition, contributed by A Hooijer and R  
725 Vernimmen, was funded by the Australian Agency for International Development and Dutch  
726 government (EMRP-BlockE, 2011), Norwegian Agency for Development Cooperation  
727 (Kampar, 2014) and United Kingdom Climate Change Unit (Berbak). K Král and M Krůček  
728 acknowledge INTER-COST project LUC23023. KK Htoo, R Farhadur, R Takeshige and Y  
729 Onoda acknowledge JSPS KAKENHI (#21H05314 & #21H02564). D Lai and OA Malik  
730 acknowledge Research Grant - Universiti Brunei Darussalam - UBD/RSCH/1.18/FICBF(b)/  
731 2023/006. D Lemke acknowledges The Nature Conservancy for access to the Sharp Bingham  
732 Mountain Preserve. J Lenoir acknowledges The Agence Nationale de la Recherche (ANR),  
733 under the framework of the young investigators' funding scheme (JCJC Grant N°ANR-19-  
734 CE32-0005-01: IMPRINT project). Iain McNicol and E Mitchard acknowledge The European  
735 Union for funding ERC grant FODEX (757526). M Milenkovic acknowledges funding from the  
736 European Union's Horizon Europe research and innovation programme under grant  
737 agreement No. 101059548. H Muller-Landau acknowledges Smithsonian ForestGEO (2023  
738 Panama lidar data). JP Ometto acknowledges the Amazon Fund/BNDES (grant 14.2.0929.1,  
739 Environmental Monitoring of Brazilian Biomes), the US Agency for International Development,  
740 Grant/ Award Number: AID-OAA-A-11-00012, as well as the support of FAPESP grant  
741 2017/22269-2. P Ploton acknowledges the support of the One Forest Vision initiative, funded  
742 by the French Ministry of Higher Education and Scientific Research and the French Ministry  
743 of Europe and Foreign Affairs. S Prober acknowledges support from the Western Australian  
744 government through its State NRM program and through Ngadju Conservation Aboriginal  
745 Corporation for the Great Western Woodlands drone-based LiDAR data. Airborne LiDAR for  
746 the Great Western Woodlands was funded through the Western Australian government  
747 through its Landgate program with further support from the Western Australian Department of

748 Biodiversity, Conservation and Attractions and Australia's Terrestrial Ecosystems Research  
749 Network. P Rana acknowledge the support of the governments of Finland and Nepal for the  
750 ForestResource Assessment (FRA) project. C Senf acknowledges the AI4Forest project  
751 (grant no. 01IS23025A) funded through the Bundesministerium für Bildung und Forschung  
752 (BMBF). A Shapiro acknowledges the support of the International Climate Initiative (IKI) of the  
753 German Federal Ministry for the Environment, Nature Conservation, Building and Nuclear  
754 Safety, and the German Development Bank KfW. G Shen acknowledges support by Natural  
755 Science Foundation of Shanghai (NSFS) (23ZR1419200), National Key R&D Program of  
756 China (NKRDP) (2024YFF1308100). M Silman acknowledges USAID/Wake Forest University  
757 Cooperative Agreement No. 7205-2721-CA-00005, NASA NISAR CAL/VAL, and the Andes-  
758 Amazon Fund. G Vincent acknowledges funding for airborne lidar data acquisitions by the  
759 French Government through various agencies and research bodies and by UK NERC in 2019.  
760 WS Wan Mohd Jaafar acknowledges Ministry of Higher Education of Malaysia (Grant no:  
761 FRGS/1/2020/WAB03/UKM/02/1). J White acknowledges the Canadian Forest Service and  
762 the Ontario Ministry of Natural Resources. Z Yuan acknowledges the National Key Research  
763 and Development Program of China (2024YFF1306501). Y Zeng acknowledges the National  
764 Key R&D Program of China (2024YFF0810500).

765

#### 766 **Competing interests**

767 A Burt and M Demol are employees and/or shareowners of Sylvera Ltd. No other competing  
768 interests declared.

769

#### 770 **Author contributions**

771 T Jucker conceived of the idea of the project. FJ Fischer and T Jucker led the data assembly  
772 and construction of the database, with assistance from J Chave, D Coomes, KC Cushman, R  
773 Dalagnol, M Dalponte, L Duncanson, S Saatchi, R Seidl, K Stereńczak and G Vaglio Laurin.  
774 FJ Fischer led the development of processing workflows and data processing, with assistance  
775 from T Jucker, B Morgan and T Jackson. FJ Fischer led the analysis and writing of a first draft

776 of the manuscript, with assistance from T Jucker, T Jackson and B Morgan. All co-authors  
777 contributed substantially through data collection, data assembly and critical revisions of the  
778 manuscript.

779

#### 780 **Data availability**

781 All openly available GCA products (87% of the database, covering 95% of the area) will be  
782 made freely available after review through the European Space Agency's Multi-Mission  
783 Algorithm and Analysis Platform (MAAP). All code and materials necessary to reproduce the  
784 analyses in this manuscript will be made publicly available on Zenodo  
785 (<https://doi.org/10.5281/zenodo.16987211>).

## 786 6 References

- 787 Almeida, D. R. A. de, Stark, S. C., Shao, G., Schietti, J., Nelson, B. W., Silva, C. A.,  
788 Gorgens, E. B., Valbuena, R., Papa, D. de A., & Brancalion, P. H. S. (2019). Optimizing  
789 the Remote Detection of Tropical Rainforest Structure with Airborne Lidar: Leaf Area  
790 Profile Sensitivity to Pulse Density and Spatial Sampling. *Remote Sensing*, *11*(1).  
791 <https://doi.org/10.3390/rs11010092>
- 792 Araujo, R. F., Grubinger, S., Celes, C. H. S., Negrón-Juárez, R. I., Garcia, M., Dandois, J.  
793 P., & Muller-Landau, H. C. (2021). Strong temporal variation in treefall and branchfall  
794 rates in a tropical forest is related to extreme rainfall: results from 5 years of monthly  
795 drone data for a 50 ha plot. *Biogeosciences*, *18*(24), 6517–6531.  
796 <https://doi.org/10.5194/bg-18-6517-2021>
- 797 Asner, G. P., Kellner, J. R., Kennedy-Bowdoin, T., Knapp, D. E., Anderson, C., & Martin, R.  
798 E. (2013). Forest Canopy Gap Distributions in the Southern Peruvian Amazon. *PLOS*  
799 *ONE*, *8*(4), e60875-. <https://doi.org/10.1371/journal.pone.0060875>
- 800 Asner, G. P., Knapp, D. E., Martin, R. E., Tupayachi, R., Anderson, C. B., Mascaro, J.,  
801 Sinca, F., Chadwick, K. D., Higgins, M., Farfan, W., Llactayo, W., & Silman, M. R.  
802 (2014). Targeted carbon conservation at national scales with high-resolution monitoring.  
803 *Proceedings of the National Academy of Sciences*, *111*(47), E5016–E5022.  
804 <https://doi.org/10.1073/pnas.1419550111>
- 805 Atkins, J. W., Bohrer, G., Fahey, R. T., Hardiman, B. S., Morin, T. H., Stovall, A. E. L.,  
806 Zimmerman, N., & Gough, C. M. (2018). Quantifying vegetation and canopy structural  
807 complexity from terrestrial LiDAR data using the forest r package. *Methods in Ecology*  
808 *and Evolution*, *9*(10), 2057–2066. [https://doi.org/https://doi.org/10.1111/2041-](https://doi.org/https://doi.org/10.1111/2041-210X.13061)  
809 [210X.13061](https://doi.org/https://doi.org/10.1111/2041-210X.13061)
- 810 Atkins, J. W., Costanza, J., Dahlin, K. M., Dannenberg, M. P., Elmore, A. J., Fitzpatrick, M.  
811 C., Hakkenberg, C. R., Hardiman, B. S., Kamoske, A., LaRue, E. A., Silva, C. A.,  
812 Stovall, A. E. L., & Tielens, E. K. (2023). Scale dependency of lidar-derived forest  
813 structural diversity. *Methods in Ecology and Evolution*, *14*(2), 708–723.  
814 <https://doi.org/https://doi.org/10.1111/2041-210X.14040>
- 815 Aubry-Kientz, M., Laybros, A., Weinstein, B., Ball, J. G. C., Jackson, T., Coomes, D., &  
816 Vincent, G. (2021). Multisensor Data Fusion for Improved Segmentation of Individual  
817 Tree Crowns in Dense Tropical Forests. *IEEE Journal of Selected Topics in Applied*  
818 *Earth Observations and Remote Sensing*, *14*, 3927–3936.  
819 <https://doi.org/10.1109/JSTARS.2021.3069159>
- 820 Battison, R., Prober, S. M., Zdunic, K., Jackson, T. D., Fischer, F. J., & Jucker, T. (2024).  
821 Tracking tree demography and forest dynamics at scale using remote sensing. *New*  
822 *Phytologist*, *244*(6), 2251–2266. <https://doi.org/https://doi.org/10.1111/nph.20199>
- 823 Beland, M., Parker, G., Sparrow, B., Harding, D., Chasmer, L., Phinn, S., Antonarakis, A., &  
824 Strahler, A. (2019). On promoting the use of lidar systems in forest ecosystem  
825 research. *Forest Ecology and Management*, *450*, 117484.  
826 <https://doi.org/https://doi.org/10.1016/j.foreco.2019.117484>
- 827 Besic, N., Picard, N., Vega, C., Bontemps, J.-D., Hertzog, L., Renaud, J.-P., Fogel, F.,  
828 Schwartz, M., Pellissier-Tanon, A., Destouet, G., Mortier, F., Planells-Rodriguez, M., &  
829 Ciais, P. (2025). Remote-sensing-based forest canopy height mapping: some models  
830 are useful, but might they provide us with even more insights when combined?

- 831 *Geoscientific Model Development*, 18(2), 337–359. <https://doi.org/10.5194/gmd-18-337->  
832 2025
- 833 Besson, M., Alison, J., Bjerger, K., Goroehowski, T. E., Høye, T. T., Jucker, T., Mann, H. M.  
834 R., & Clements, C. F. (2022). Towards the fully automated monitoring of ecological  
835 communities. *Ecology Letters*, 25(12), 2753–2775.  
836 <https://doi.org/https://doi.org/10.1111/ele.14123>
- 837 Blois, J. L., Williams, J. W., Fitzpatrick, M. C., Jackson, S. T., & Ferrier, S. (2013). Space  
838 can substitute for time in predicting climate-change effects on biodiversity. *Proceedings*  
839 *of the National Academy of Sciences*, 110(23), 9374–9379.  
840 <https://doi.org/10.1073/pnas.1220228110>
- 841 Brandt, M., Tucker, C. J., Kariyaa, A., Rasmussen, K., Abel, C., Small, J., Chave, J.,  
842 Rasmussen, L. V., Hiernaux, P., Diouf, A. A., Kergoat, L., Mertz, O., Igel, C., Gieseke,  
843 F., Schöning, J., Li, S., Melocik, K., Meyer, J., Sinno, S., ... Fensholt, R. (2020). An  
844 unexpectedly large count of trees in the West African Sahara and Sahel. *Nature*,  
845 587(7832), 78–82. <https://doi.org/10.1038/s41586-020-2824-5>
- 846 Bürkner, P. C. (2018). Advanced Bayesian multilevel modeling with the R package brms. *R*  
847 *Journal*, 10(1), 395–411. <https://doi.org/10.32614/rj-2018-017>
- 848 Cao, L., Coops, N. C., Innes, J. L., Sheppard, S. R. J., Fu, L., Ruan, H., & She, G. (2016).  
849 Estimation of forest biomass dynamics in subtropical forests using multi-temporal  
850 airborne LiDAR data. *Remote Sensing of Environment*, 178, 158–171.  
851 <https://doi.org/https://doi.org/10.1016/j.rse.2016.03.012>
- 852 Coops, N. C., Tompalski, P., Goodbody, T. R. H., Queinnec, M., Luther, J. E., Bolton, D. K.,  
853 White, J. C., Wulder, M. A., van Lier, O. R., & Hermosilla, T. (2021). Modelling lidar-  
854 derived estimates of forest attributes over space and time: A review of approaches and  
855 future trends. *Remote Sensing of Environment*, 260, 112477.  
856 <https://doi.org/https://doi.org/10.1016/j.rse.2021.112477>
- 857 Cushman, K. C., Detto, M., García, M., & Muller-Landau, H. C. (2022). Soils and topography  
858 control natural disturbance rates and thereby forest structure in a lowland tropical  
859 landscape. *Ecology Letters*, 25(5), 1126–1138. <https://doi.org/10.1111/ele.13978>
- 860 Dalagnol, R., Wagner, F. H., Galvão, L. S., Streher, A. S., Phillips, O. L., Gloor, E., Pugh, T.  
861 A. M., Ometto, J. P. H. B., & Aragão, L. E. O. C. (2021). Large-scale variations in the  
862 dynamics of Amazon forest canopy gaps from airborne lidar data and opportunities for  
863 tree mortality estimates. *Scientific Reports*, 11(1), 1388. [https://doi.org/10.1038/s41598-](https://doi.org/10.1038/s41598-020-80809-w)  
864 020-80809-w
- 865 Davies, A. B., & Asner, G. P. (2014). Advances in animal ecology from 3D-LiDAR ecosystem  
866 mapping. *Trends in Ecology & Evolution*, 29(12), 681–691.  
867 <https://doi.org/10.1016/j.tree.2014.10.005>
- 868 de Angeli Dutra, D., Erikson, A., Genes, L., Dirzo, R., & Venturini, A. M. (2025). Elevating  
869 local perspectives for equity in ecological research. *Trends in Ecology & Evolution*,  
870 40(5), 415–418. <https://doi.org/https://doi.org/10.1016/j.tree.2025.03.006>
- 871 de Lima, R. A. F., Phillips, O. L., Duque, A., Tello, J. S., Davies, S. J., de Oliveira, A. A.,  
872 Muller, S., Honorio Coronado, E. N., Vilanova, E., Cuni-Sanchez, A., Baker, T. R.,  
873 Ryan, C. M., Malizia, A., Lewis, S. L., ter Steege, H., Ferreira, J., Marimon, B. S., Luu,  
874 H. T., Imani, G., ... Vásquez, R. (2022). Making forest data fair and open. *Nature*  
875 *Ecology & Evolution*, 6(6), 656–658. <https://doi.org/10.1038/s41559-022-01738-7>
- 876 Denslow, J. S. (1987). Tropical Rainforest Gaps and Tree Species Diversity. *Annual Review*  
877 *of Ecology and Systematics*, 18, 431–451.  
878 <http://www.jstor.org/brs.idm.oclc.org/stable/2097139>

- 879 Didan, K. (2025, March 16). *MODIS/Terra Vegetation Indices Monthly L3 Global 0.05Deg*  
880 *CMG V061 [Data set]*. NASA EOSDIS Land Processes Distributed Active Archive  
881 Center.
- 882 Dinerstein, E., Olson, D., Joshi, A., Vynne, C., Burgess, N. D., Wikramanayake, E., Hahn,  
883 N., Palminteri, S., Hedao, P., Noss, R., Hansen, M., Locke, H., Ellis, E. C., Jones, B.,  
884 Barber, C. V., Hayes, R., Kormos, C., Martin, V., Crist, E., ... Saleem, M. (2017). An  
885 Ecoregion-Based Approach to Protecting Half the Terrestrial Realm. *BioScience*, *67*(6),  
886 534–545. <https://doi.org/10.1093/biosci/bix014>
- 887 Dowle, M., & Srinivasan, A. (2025). *data.table: Extension of `data.frame`*. [https://CRAN.R-](https://CRAN.R-project.org/package=data.table)  
888 [project.org/package=data.table](https://CRAN.R-project.org/package=data.table)
- 889 Eitel, J. U. H., Höfle, B., Vierling, L. A., Abellán, A., Asner, G. P., Deems, J. S., Glennie, C.  
890 L., Joerg, P. C., LeWinter, A. L., Magney, T. S., Mandlburger, G., Morton, D. C., Müller,  
891 J., & Vierling, K. T. (2016). Beyond 3-D: The new spectrum of lidar applications for  
892 earth and ecological sciences. *Remote Sensing of Environment*, *186*, 372–392.  
893 <https://doi.org/https://doi.org/10.1016/j.rse.2016.08.018>
- 894 European Space Agency. (2024). *Copernicus Global Digital Elevation Model. Distributed by*  
895 *OpenTopography*.
- 896 Fassnacht, F. E., White, J. C., Wulder, M. A., & Næsset, E. (2024). Remote sensing in  
897 forestry: current challenges, considerations and directions. *Forestry: An International*  
898 *Journal of Forest Research*, *97*(1), 11–37. <https://doi.org/10.1093/forestry/cpad024>
- 899 Fick, S. E., & Hijmans, R. J. (2017). WorldClim 2: new 1-km spatial resolution climate  
900 surfaces for global land areas. *International Journal of Climatology*, *37*(12), 4302–4315.  
901 <https://doi.org/10.1002/joc.5086>
- 902 Fischer, F. J., Jackson, T., Vincent, G., & Jucker, T. (2024). Robust characterisation of forest  
903 structure from airborne laser scanning—A systematic assessment and sample workflow  
904 for ecologists. *Methods in Ecology and Evolution*, *15*(10), 1873–1888.  
905 <https://doi.org/https://doi.org/10.1111/2041-210X.14416>
- 906 Fischer, F. J., & Jucker, T. (2024). No evidence for fractal scaling in canopy surfaces across  
907 a diverse range of forest types. *Journal of Ecology*, *112*(3), 470–486.  
908 <https://doi.org/https://doi.org/10.1111/1365-2745.14244>
- 909 Fischer, F. J., Labrière, N., Vincent, G., Hérault, B., Alonso, A., Memiaghe, H., Bissiengou,  
910 P., Kenfack, D., Saatchi, S., & Chave, J. (2020). A simulation method to infer tree  
911 allometry and forest structure from airborne laser scanning and forest inventories.  
912 *Remote Sensing of Environment*, *251*, 112056.  
913 <https://doi.org/https://doi.org/10.1016/j.rse.2020.112056>
- 914 Franklin, J. F., Shugart, H. H., & Harmon, M. E. (1987). Tree death as an ecological process.  
915 *BioScience*, *37*(8), 550–556. <https://doi.org/10.2307/1310665>
- 916 Frelich, L. E., Jöggiste, K., Stanturf, J. A., Parro, K., & Baders, E. (2018). Natural  
917 Disturbances and Forest Management: Interacting Patterns on the Landscape. In A. H.  
918 Perera, U. Peterson, G. M. Pastur, & L. R. Iverson (Eds.), *Ecosystem Services from*  
919 *Forest Landscapes: Broadscale Considerations* (pp. 221–248). Springer International  
920 Publishing. [https://doi.org/10.1007/978-3-319-74515-2\\_8](https://doi.org/10.1007/978-3-319-74515-2_8)
- 921 Gillespie, C. S. (2015). Fitting Heavy Tailed Distributions: The powerLaw Package. *Journal*  
922 *of Statistical Software*, *64*(2), 1–16. <http://www.jstatsoft.org/v64/i02/>
- 923 Gonzalez, A., Vihervaara, P., Balvanera, P., Bates, A. E., Bayraktarov, E., Bellingham, P. J.,  
924 Bruder, A., Campbell, J., Catchen, M. D., Cavender-Bares, J., Chase, J., Coops, N.,  
925 Costello, M. J., Czócz, B., Delavaud, A., Dornelas, M., Dubois, G., Duffy, E. J.,  
926 Eggermont, H., ... Torrelío, C. Z. (2023). A global biodiversity observing system to unite

- 927 monitoring and guide action. *Nature Ecology & Evolution*, 7(12), 1947–1952.  
928 <https://doi.org/10.1038/s41559-023-02171-0>
- 929 Goodbody, T. R. H., Tompalski, P., Coops, N. C., White, J. C., Wulder, M. A., & Sanelli, M.  
930 (2020). Uncovering spatial and ecological variability in gap size frequency distributions  
931 in the Canadian boreal forest. *Scientific Reports*, 10(1), 6069.  
932 <https://doi.org/10.1038/s41598-020-62878-z>
- 933 Gril, E., Laslier, M., Gallet-Moron, E., Durrieu, S., Spicher, F., Le Roux, V., Brasseur, B.,  
934 Haesen, S., Van Meerbeek, K., Decocq, G., Marrec, R., & Lenoir, J. (2023). Using  
935 airborne LiDAR to map forest microclimate temperature buffering or amplification.  
936 *Remote Sensing of Environment*, 298, 113820.  
937 <https://doi.org/https://doi.org/10.1016/j.rse.2023.113820>
- 938 Hanel, R., Corominas-Murtra, B., Liu, B., & Thurner, S. (2017). Fitting power-laws in  
939 empirical data with estimators that work for all exponents. *PLOS ONE*, 12(2), 1–15.  
940 <https://doi.org/10.1371/journal.pone.0170920>
- 941 Heiskanen, J., Haurinen, H., Wekesa, C., & Pellikka, P. (2024). Repeat airborne laser  
942 scanning to assess canopy height changes in tropical montane forests. *ISPRS Ann.*  
943 *Photogramm. Remote Sens. Spatial Inf. Sci.*, X-3–2024, 179–185.  
944 <https://doi.org/10.5194/isprs-annals-X-3-2024-179-2024>
- 945 Hijmans, R. J. (2025). *terra: Spatial Data Analysis*. [https://CRAN.R-](https://CRAN.R-project.org/package=terra)  
946 [project.org/package=terra](https://CRAN.R-project.org/package=terra)
- 947 Huertas, C., Sabatier, D., Derroire, G., Ferry, B., Jackson, Toby. D., Péliissier, R., & Vincent,  
948 G. (2022). Mapping tree mortality rate in a tropical moist forest using multi-temporal  
949 LiDAR. *International Journal of Applied Earth Observation and Geoinformation*, 109,  
950 102780. <https://doi.org/https://doi.org/10.1016/j.jag.2022.102780>
- 951 Humboldt, A. von. (1801). Briefe des Herrn Alexander von Humboldt. *Neue Berlinische*  
952 *Monatschrift*, 115–141.
- 953 Hunter, M. O., Keller, M., Morton, D., Cook, B., Lefsky, M., Ducey, M., Saleska, S., de  
954 Oliveira Jr, R. C., & Schiatti, J. (2015). Structural Dynamics of Tropical Moist Forest  
955 Gaps. *PLOS ONE*, 10(7), 1–19. <https://doi.org/10.1371/journal.pone.0132144>
- 956 Jackson, T. D., Fischer, F. J., Vincent, G., Gorgens, E. B., Keller, M., Chave, J., Jucker, T.,  
957 & Coomes, D. A. (2024). Tall Bornean forests experience higher canopy disturbance  
958 rates than those in the eastern Amazon or Guiana shield. *Global Change Biology*,  
959 30(9), e17493. <https://doi.org/https://doi.org/10.1111/gcb.17493>
- 960 Jarron, L. R., Coops, N. C., MacKenzie, W. H., Tompalski, P., & Dykstra, P. (2020).  
961 Detection of sub-canopy forest structure using airborne LiDAR. *Remote Sensing of*  
962 *Environment*, 244, 111770. <https://doi.org/https://doi.org/10.1016/j.rse.2020.111770>
- 963 Joerg, P. C., Morsdorf, F., & Zemp, M. (2012). Uncertainty assessment of multi-temporal  
964 airborne laser scanning data: A case study on an Alpine glacier. *Remote Sensing of*  
965 *Environment*, 127, 118–129. <https://doi.org/https://doi.org/10.1016/j.rse.2012.08.012>
- 966 Jucker, T. (2022). Deciphering the fingerprint of disturbance on the three-dimensional  
967 structure of the world's forests. *New Phytologist*, 233(2), 612–617.  
968 <https://doi.org/https://doi.org/10.1111/nph.17729>
- 969 Jucker, T., Fischer, F. J., Chave, J., Coomes, D. A., Caspersen, J., Ali, A., Loubota Panzou,  
970 G. J., Feldpausch, T. R., Falster, D., Usoltsev, V. A., Adu-Bredu, S., Alves, L. F.,  
971 Aminpour, M., Angoboy, I. B., Anten, N. P. R., Antin, C., Askari, Y., Muñoz, R.,  
972 Ayyappan, N., ... Zavala, M. A. (2022). Tallo: A global tree allometry and crown  
973 architecture database. *Global Change Biology*, 28(17).  
974 <https://doi.org/10.1111/gcb.16302>

- 975 Kampe, T. U. (2010). NEON: the first continental-scale ecological observatory with airborne  
976 remote sensing of vegetation canopy biochemistry and structure. *Journal of Applied*  
977 *Remote Sensing*, 4(1), 043510. <https://doi.org/10.1117/1.3361375>
- 978 Karan, M., Liddell, M., Prober, S. M., Arndt, S., Beringer, J., Boer, M., Cleverly, J., Eamus,  
979 D., Grace, P., Van Gorsel, E., Hero, J.-M., Hutley, L., Macfarlane, C., Metcalfe, D.,  
980 Meyer, W., Pendall, E., Sebastian, A., & Wardlaw, T. (2016). The Australian SuperSite  
981 Network: A continental, long-term terrestrial ecosystem observatory. *Science of The*  
982 *Total Environment*, 568, 1263–1274. <https://doi.org/10.1016/j.scitotenv.2016.05.170>
- 983 Karger, D. N., Conrad, O., Böhner, J., Kawohl, T., Kreft, H., Soria-Auza, R. W.,  
984 Zimmermann, N. E., Linder, H. P., & Kessler, M. (2017). Climatologies at high  
985 resolution for the earth's land surface areas. *Scientific Data*, 4(1), 170122.  
986 <https://doi.org/10.1038/sdata.2017.122>
- 987 Kellner, J. R., & Asner, G. P. (2009). Convergent structural responses of tropical forests to  
988 diverse disturbance regimes. *Ecology Letters*, 12(9), 887–897.  
989 <https://doi.org/https://doi.org/10.1111/j.1461-0248.2009.01345.x>
- 990 Kellogg, K., Hoffman, P., Standley, S., Shaffer, S., Rosen, P., Edelstein, W., Dunn, C.,  
991 Baker, C., Barela, P., Shen, Y., Guerrero, A. M., Xaypraseuth, P., Sagi, V. R.,  
992 Sreekantha, C. V., Harinath, N., Kumar, R., Bhan, R., & Sarma, C. V. H. S. (2020).  
993 NASA-ISRO Synthetic Aperture Radar (NISAR) Mission. *2020 IEEE Aerospace*  
994 *Conference*, 1–21. <https://doi.org/10.1109/AERO47225.2020.9172638>
- 995 Khosravipour, A., Skidmore, A. K., & Isenburg, M. (2016). Generating spike-free digital  
996 surface models using LiDAR raw point clouds: A new approach for forestry applications.  
997 *International Journal of Applied Earth Observation and Geoinformation*, 52, 104–114.  
998 <https://doi.org/https://doi.org/10.1016/j.jag.2016.06.005>
- 999 Kissling, W. D., & Shi, Y. (2023). Which metrics derived from airborne laser scanning are  
1000 essential to measure the vertical profile of ecosystems? *Diversity and Distributions*,  
1001 29(10), 1315–1320. <https://doi.org/https://doi.org/10.1111/ddi.13760>
- 1002 Knapp, N., Fischer, R., Cazcarra-Bes, V., & Huth, A. (2020). Structure metrics to generalize  
1003 biomass estimation from lidar across forest types from different continents. *Remote*  
1004 *Sensing of Environment*, 237, 111597.  
1005 <https://doi.org/https://doi.org/10.1016/j.rse.2019.111597>
- 1006 Kohyama, T. S., Kohyama, T. I., & Sheil, D. (2018). Definition and estimation of vital rates  
1007 from repeated censuses: Choices, comparisons and bias corrections focusing on trees.  
1008 *Methods in Ecology and Evolution*, 9(4), 809–821.  
1009 <https://doi.org/https://doi.org/10.1111/2041-210X.12929>
- 1010 Kohyama, T. S., Kohyama, T. I., & Sheil, D. (2019). Estimating net biomass production and  
1011 loss from repeated measurements of trees in forests and woodlands: Formulae, biases  
1012 and recommendations. *Forest Ecology and Management*, 433, 729–740.  
1013 <https://doi.org/https://doi.org/10.1016/j.foreco.2018.11.010>
- 1014 Körner, C. (2003). Slow in, Rapid out—Carbon Flux Studies and Kyoto Targets. *Science*,  
1015 300(5623), 1242–1243. <https://doi.org/10.1126/science.1084460>
- 1016 Krüger, K., Senf, C., Jucker, T., Pflugmacher, D., & Seidl, R. (2024). Gap expansion is the  
1017 dominant driver of canopy openings in a temperate mountain forest landscape. *Journal*  
1018 *of Ecology*, 112(7), 1501–1515. <https://doi.org/https://doi.org/10.1111/1365-2745.14320>
- 1019 Lang, N., Jetz, W., Schindler, K., & Wegner, J. D. (2023). A high-resolution canopy height  
1020 model of the Earth. *Nature Ecology & Evolution*, 7(11), 1778–1789.  
1021 <https://doi.org/10.1038/s41559-023-02206-6>

- 1022 LaRue, E. A., Fahey, R., Fuson, T. L., Foster, J. R., Matthes, J. H., Krause, K., & Hardiman,  
1023 B. S. (2022). Evaluating the sensitivity of forest structural diversity characterization to  
1024 LiDAR point density. *Ecosphere*, *13*(9), e4209.  
1025 <https://doi.org/https://doi.org/10.1002/ecs2.4209>
- 1026 Leitold, V., Morton, D. C., Longo, M., dos-Santos, M. N., Keller, M., & Scaranello, M. (2018).  
1027 El Niño drought increased canopy turnover in Amazon forests. *New Phytologist*, *219*(3),  
1028 959–971. <https://doi.org/https://doi.org/10.1111/nph.15110>
- 1029 Lenoir, J., Gril, E., Durrieu, S., Horen, H., Laslier, M., Lembrechts, J. J., Zellweger, F.,  
1030 Alleaume, S., Brasseur, B., Buridant, J., Dayal, K., De Frenne, P., Gallet-Moron, E.,  
1031 Marrec, R., Meeussen, C., Rocchini, D., Van Meerbeek, K., & Decocq, G. (2022).  
1032 Unveil the unseen: Using LiDAR to capture time-lag dynamics in the herbaceous layer  
1033 of European temperate forests. *Journal of Ecology*, *110*(2), 282–300.
- 1034 Lines, E. R., Fischer, F. J., Owen, H. J. F., & Jucker, T. (2022). The shape of trees:  
1035 Reimagining forest ecology in three dimensions with remote sensing. *Journal of*  
1036 *Ecology*, *110*(8). <https://doi.org/10.1111/1365-2745.13944>
- 1037 Liu, S., Brandt, M., Nord-Larsen, T., Chave, J., Reiner, F., Lang, N., Tong, X., Ciais, P., Igel,  
1038 C., Pascual, A., Guerra-Hernandez, J., Li, S., Mugabowindekwe, M., Saatchi, S., Yue,  
1039 Y., Chen, Z., & Fensholt, R. (2025). The overlooked contribution of trees outside forests  
1040 to tree cover and woody biomass across Europe. *Science Advances*, *9*(37), eadh4097.  
1041 <https://doi.org/10.1126/sciadv.adh4097>
- 1042 Lobo, E., & Dalling, J. W. (2014). Spatial scale and sampling resolution affect measures of  
1043 gap disturbance in a lowland tropical forest: implications for understanding forest  
1044 regeneration and carbon storage. *Proceedings of the Royal Society B: Biological*  
1045 *Sciences*, *281*(1778), 20133218. <https://doi.org/10.1098/rspb.2013.3218>
- 1046 Loke, L. H. L., & Chisholm, R. A. (2022). Measuring habitat complexity and spatial  
1047 heterogeneity in ecology. *Ecology Letters*, *25*(10), 2269–2288.  
1048 <https://doi.org/10.1111/ele.14084>
- 1049 Melendy, L., Hagen, S. C., Sullivan, F. B., Pearson, T. R. H., Walker, S. M., Ellis, P., Kustiyo,  
1050 Sambodo, A. K., Roswintarti, O., Hanson, M. A., Klassen, A. W., Palace, M. W.,  
1051 Braswell, B. H., & Delgado, G. M. (2018). Automated method for measuring the extent  
1052 of selective logging damage with airborne LiDAR data. *ISPRS Journal of*  
1053 *Photogrammetry and Remote Sensing*, *139*, 228–240.  
1054 <https://doi.org/https://doi.org/10.1016/j.isprsjprs.2018.02.022>
- 1055 Moudrý, V., Remelgado, R., Forkel, M., Torresani, M., Laurin, G. V., Sarovcova, E., Millan,  
1056 V. E. G., Fischer, F. J., Jucker, T., Gallay, M., Kacic, P., Hakkenberg, C. R., Kokalj, Ž.,  
1057 Stereńczak, K., Erfanifard, Y., Rocchini, D., Prošek, J., Roilo, S., Gdulova, K., ...  
1058 Barták, V. (2024). Harmonised airborne laser scanning products can address the  
1059 limitations of large-scale spaceborne vegetation mapping [pre-print]. *EarthArXiv*.  
1060 <https://doi.org/10.31223/X5D70J>
- 1061 Mutanga, O., Masenyama, A., & Sibanda, M. (2023). Spectral saturation in the remote  
1062 sensing of high-density vegetation traits: A systematic review of progress, challenges,  
1063 and prospects. *ISPRS Journal of Photogrammetry and Remote Sensing*, *198*, 297–309.  
1064 <https://doi.org/https://doi.org/10.1016/j.isprsjprs.2023.03.010>
- 1065 Næsset, E. (2002). Predicting forest stand characteristics with airborne scanning laser using  
1066 a practical two-stage procedure and field data. *Remote Sensing of Environment*, *80*(1),  
1067 88–99. [https://doi.org/10.1016/S0034-4257\(01\)00290-5](https://doi.org/10.1016/S0034-4257(01)00290-5)
- 1068 Næsset, E. (2005). Assessing sensor effects and effects of leaf-off and leaf-on canopy  
1069 conditions on biophysical stand properties derived from small-footprint airborne laser

- 1070 data. *Remote Sensing of Environment*, 98(2), 356–370.  
1071 <https://doi.org/https://doi.org/10.1016/j.rse.2005.07.012>
- 1072 Næsset, E. (2009). Effects of different sensors, flying altitudes, and pulse repetition  
1073 frequencies on forest canopy metrics and biophysical stand properties derived from  
1074 small-footprint airborne laser data. *Remote Sensing of Environment*, 113(1), 148–159.  
1075 <https://doi.org/https://doi.org/10.1016/j.rse.2008.09.001>
- 1076 Næsset, E., Bollandsås, O. M., Gobakken, T., Gregoire, T. G., & Ståhl, G. (2013). Model-  
1077 assisted estimation of change in forest biomass over an 11year period in a sample  
1078 survey supported by airborne LiDAR: A case study with post-stratification to provide  
1079 “activity data”. *Remote Sensing of Environment*, 128, 299–314.  
1080 <https://doi.org/https://doi.org/10.1016/j.rse.2012.10.008>
- 1081 Næsset, E., Gobakken, T., Holmgren, J., Hyypä, H., Hyypä, J., Maltamo, M., Nilsson, M.,  
1082 Olsson, H., Persson, Å., & Söderman, U. (2004). Laser scanning of forest resources:  
1083 the nordic experience. *Scandinavian Journal of Forest Research*, 19(6), 482–499.  
1084 <https://doi.org/10.1080/02827580410019553>
- 1085 Nelson, R. (2013). How did we get here? An early history of forestry lidar. *Canadian Journal*  
1086 *of Remote Sensing*, 39, S6–S17. <https://doi.org/10.5589/m13-011>
- 1087 Newman, M. E. J. (2005). Power laws, Pareto distributions and Zipf’s law. *Contemporary*  
1088 *Physics*, 46(5), 323–351. <https://doi.org/10.1080/00107510500052444>
- 1089 Okyay, U., Telling, J., Glennie, C. L., & Dietrich, W. E. (2019). Airborne lidar change  
1090 detection: An overview of Earth sciences applications. *Earth-Science Reviews*, 198,  
1091 102929. <https://doi.org/https://doi.org/10.1016/j.earscirev.2019.102929>
- 1092 Ometto, J. P., Gorgens, E. B., de Souza Pereira, F. R., Sato, L., de Assis, M. L. R.,  
1093 Cantinho, R., Longo, M., Jacon, A. D., & Keller, M. (2023). A biomass map of the  
1094 Brazilian Amazon from multisource remote sensing. *Scientific Data*, 10(1), 668.  
1095 <https://doi.org/10.1038/s41597-023-02575-4>
- 1096 Paulsen, J., & Körner, C. (2014). A climate-based model to predict potential treeline position  
1097 around the globe. *Alpine Botany*, 124(1), 1–12. [https://doi.org/10.1007/s00035-014-](https://doi.org/10.1007/s00035-014-0124-0)  
1098 0124-0
- 1099 Pebesma, E. (2018). Simple Features for R: Standardized Support for Spatial Vector Data.  
1100 *The R Journal*, 10(1), 439–446. <https://doi.org/10.32614/RJ-2018-009>
- 1101 Ploton, P., Mortier, F., Réjou-Méchain, M., Barbier, N., Picard, N., Rossi, V., Dormann, C.,  
1102 Cornu, G., Viennois, G., Bayol, N., Lyapustin, A., Gourlet-Fleury, S., & Pélissier, R.  
1103 (2020). Spatial validation reveals poor predictive performance of large-scale ecological  
1104 mapping models. *Nature Communications*, 11(1). [https://doi.org/10.1038/s41467-020-](https://doi.org/10.1038/s41467-020-18321-y)  
1105 18321-y
- 1106 Potapov, P., Hansen, M. C., Laestadius, L., Turubanova, S., Yaroshenko, A., Thies, C.,  
1107 Smith, W., Zhuravleva, I., Komarova, A., Minnemeyer, S., & Esipova, E. (2017). The  
1108 last frontiers of wilderness: Tracking loss of intact forest landscapes from 2000 to 2013.  
1109 *Science Advances*, 3, e1600821. <https://doi.org/10.1126/sciadv.1600821>
- 1110 Potapov, P., Hansen, M. C., Pickens, A., Hernandez-Serna, A., Tyukavina, A., Turubanova,  
1111 S., Zalles, V., Li, X., Khan, A., Stolle, F., Harris, N., Song, X.-P., Baggett, A.,  
1112 Kommareddy, I., & Kommareddy, A. (2022). The Global 2000-2020 Land Cover and  
1113 Land Use Change Dataset Derived From the Landsat Archive: First Results. *Frontiers*  
1114 *in Remote Sensing*, 3. [https://www.frontiersin.org/journals/remote-](https://www.frontiersin.org/journals/remote-sensing/articles/10.3389/frsen.2022.856903)  
1115 sensing/articles/10.3389/frsen.2022.856903
- 1116 Potapov, P., Li, X., Hernandez-Serna, A., Tyukavina, A., Hansen, M. C., Kommareddy, A.,  
1117 Pickens, A., Turubanova, S., Tang, H., Silva, C. E., Armston, J., Dubayah, R., Blair, J.

- 1118 B., & Hofton, M. (2021). Mapping global forest canopy height through integration of  
1119 GEDI and Landsat data. *Remote Sensing of Environment*, 253, 112165.  
1120 <https://doi.org/https://doi.org/10.1016/j.rse.2020.112165>
- 1121 Quan, Y., Li, M., Hao, Y., & Wang, B. (2021). Comparison and Evaluation of Different Pit-  
1122 Filling Methods for Generating High Resolution Canopy Height Model Using UAV Laser  
1123 Scanning Data. *Remote Sensing*, 13(12). <https://doi.org/10.3390/rs13122239>
- 1124 Quegan, S., Le Toan, T., Chave, J., Dall, J., Exbrayat, J. F., Minh, D. H. T., Lomas, M.,  
1125 D'Alessandro, M. M., Paillou, P., Papathanassiou, K., Rocca, F., Saatchi, S., Scipal, K.,  
1126 Shugart, H., Smallman, T. L., Soja, M. J., Tebaldini, S., Ulander, L., Villard, L., &  
1127 Williams, M. (2019). The European Space Agency BIOMASS mission: Measuring forest  
1128 above-ground biomass from space. *Remote Sensing of Environment*, 227, 44–60.  
1129 <https://doi.org/10.1016/j.rse.2019.03.032>
- 1130 Reis, C. R., Jackson, T. D., Gorgens, E. B., Dalagnol, R., Jucker, T., Nunes, M. H., Ometto,  
1131 J. P., Aragão, L. E. O. C., Rodriguez, L. C. E., & Coomes, D. A. (2022). Forest  
1132 disturbance and growth processes are reflected in the geographical distribution of large  
1133 canopy gaps across the Brazilian Amazon. *Journal of Ecology*, 110(12), 2971–2983.  
1134 <https://doi.org/https://doi.org/10.1111/1365-2745.14003>
- 1135 Riofrío, J., White, J. C., Tompalski, P., Coops, N. C., & Wulder, M. A. (2022). Harmonizing  
1136 multi-temporal airborne laser scanning point clouds to derive periodic annual height  
1137 increments in temperate mixedwood forests. *Canadian Journal of Forest Research*,  
1138 52(10), 1334–1352. <https://doi.org/10.1139/cjfr-2022-0055>
- 1139 Ritter, E., Dalsgaard, L., & Einhorn, K. S. (2005). Light, temperature and soil moisture  
1140 regimes following gap formation in a semi-natural beech-dominated forest in Denmark.  
1141 *Forest Ecology and Management*, 206(1), 15–33.  
1142 <https://doi.org/https://doi.org/10.1016/j.foreco.2004.08.011>
- 1143 Rosen, A., Jörg Fischer, F., Coomes, D. A., Jackson, T. D., Asner, G. P., & Jucker, T.  
1144 (2024). Tracking shifts in forest structural complexity through space and time in human-  
1145 modified tropical landscapes. *Ecography*, n/a(n/a), e07377.  
1146 <https://doi.org/https://doi.org/10.1111/ecog.07377>
- 1147 Roussel, J.-R., Auty, D., Coops, N. C., Tompalski, P., Goodbody, T. R. H., Meador, A. S.,  
1148 Bourdon, J.-F., de Boissieu, F., & Achim, A. (2020). lidR: An R package for analysis of  
1149 Airborne Laser Scanning (ALS) data. *Remote Sensing of Environment*, 251, 112061.  
1150 <https://doi.org/https://doi.org/10.1016/j.rse.2020.112061>
- 1151 Roussel, J.-R., Caspersen, J., Béland, M., Thomas, S., & Achim, A. (2017). Removing bias  
1152 from LiDAR-based estimates of canopy height: Accounting for the effects of pulse  
1153 density and footprint size. *Remote Sensing of Environment*, 198, 1–16.  
1154 <https://doi.org/https://doi.org/10.1016/j.rse.2017.05.032>
- 1155 Saatchi, S. S., & Favrichon, S. (2023). *Global Vegetation Height Metrics from GEDI and*  
1156 *ICESat2*. ORNL DAAC. <https://doi.org/10.3334/ORNLDAAAC/2294>
- 1157 Schwalb-Willmann, J. (2024). *basemaps: Accessing Spatial Basemaps in R*.  
1158 <https://CRAN.R-project.org/package=basemaps>
- 1159 Schwartz, M., Ciais, P., De Truchis, A., Chave, J., Otlé, C., Vega, C., Wigneron, J.-P.,  
1160 Nicolas, M., Jouaber, S., Liu, S., Brandt, M., & Fayad, I. (2023). FORMS: Forest  
1161 Multiple Source height, wood volume, and biomass maps in France at 10 to 30m  
1162 resolution based on Sentinel-1, Sentinel-2, and Global Ecosystem Dynamics  
1163 Investigation (GEDI) data with a deep learning approach. *Earth System Science Data*,  
1164 15(11), 4927–4945. <https://doi.org/10.5194/essd-15-4927-2023>

- 1165 Senf, C. (2022). Seeing the System from Above: The Use and Potential of Remote Sensing  
1166 for Studying Ecosystem Dynamics. *Ecosystems*, 25(8), 1719–1737.  
1167 <https://doi.org/10.1007/s10021-022-00777-2>
- 1168 Shugart, H. H., Asner, G. P., Fischer, R., Huth, A., Knapp, N., Le Toan, T., & Shuman, J. K.  
1169 (2015). Computer and remote-sensing infrastructure to enhance large-scale testing of  
1170 individual-based forest models. *Frontiers in Ecology and the Environment*, 13(9), 503–  
1171 511. <https://doi.org/10.1890/140327>
- 1172 Shugart, H. H., Saatchi, S., & Hall, F. G. (2010). Importance of structure and its  
1173 measurement in quantifying function of forest ecosystems. *Journal of Geophysical*  
1174 *Research: Biogeosciences*, 115(G2), n/a-n/a. <https://doi.org/10.1029/2009JG000993>
- 1175 Simard, M., Pinto, N., Fisher, J. B., & Baccini, A. (2011). Mapping forest canopy height  
1176 globally with spaceborne lidar. *Journal of Geophysical Research: Biogeosciences*,  
1177 116(G4). <https://doi.org/10.1029/2011JG001708>
- 1178 Spriggs, R. A., Vanderwel, M. C., Jones, T. A., Caspersen, J. P., & Coomes, D. A. (2015). A  
1179 simple area-based model for predicting airborne LiDAR first returns from stem diameter  
1180 distributions: An example study in an uneven-aged, mixed temperate forest. *Canadian*  
1181 *Journal of Forest Research*, 45(10), 1338–1350. <https://doi.org/10.1139/cjfr-2015-0018>
- 1182 Staver, A. C., Archibald, S., & Levin, S. A. (2011). The Global Extent and Determinants of  
1183 Savanna and Forest as Alternative Biome States. *Science*, 334(6053), 230–232.  
1184 <https://doi.org/10.1126/science.1210465>
- 1185 Stereńczak, K., Ciesielski, M., Balazy, R., & Zawila-Niedźwiecki, T. (2016). Comparison of  
1186 various algorithms for DTM interpolation from LIDAR data in dense mountain forests.  
1187 *European Journal of Remote Sensing*, 49(1), 599–621.  
1188 <https://doi.org/10.5721/EuJRS20164932>
- 1189 Stereńczak, K., Laurin, G. V., Chirici, G., Coomes, D. A., Dalponte, M., Latifi, H., & Puletti, N.  
1190 (2020). Global Airborne Laser Scanning Data Providers Database (GlobALS)—A New  
1191 Tool for Monitoring Ecosystems and Biodiversity. *Remote Sensing*, 12(11).  
1192 <https://doi.org/10.3390/rs12111877>
- 1193 Tao, S., Guo, Q., Li, C., Wang, Z., & Fang, J. (2016). Global patterns and determinants of  
1194 forest canopy height. *Ecology*, 97(12), 3265–3270.  
1195 <https://doi.org/10.1002/ecy.1580>
- 1196 Taubert, F., Hartig, F., Dobner, H.-J., & Huth, A. (2013). On the Challenge of Fitting Tree  
1197 Size Distributions in Ecology. *PLOS ONE*, 8(2), e58036-  
1198 <https://doi.org/10.1371/journal.pone.0058036>
- 1199 Taubert, F., Jahn, M. W., Dobner, H.-J., Wiegand, T., & Huth, A. (2015). The structure of  
1200 tropical forests and sphere packings. *Proceedings of the National Academy of*  
1201 *Sciences*, 112(49), 15125–15129. <https://doi.org/10.1073/pnas.1513417112>
- 1202 Toivonen, J., Kangas, A., Maltamo, M., Kukkonen, M., & Packalen, P. (2023). Assessing  
1203 biodiversity using forest structure indicators based on airborne laser scanning data.  
1204 *Forest Ecology and Management*, 546, 121376.  
1205 <https://doi.org/10.1016/j.foreco.2023.121376>
- 1206 Tolan, J., Yang, H.-I., Nosarzewski, B., Couairon, G., Vo, H. V., Brandt, J., Spore, J.,  
1207 Majumdar, S., Haziza, D., Vamaraju, J., Moutakanni, T., Bojanowski, P., Johns, T.,  
1208 White, B., Tiecke, T., & Couprie, C. (2024). Very high resolution canopy height maps  
1209 from RGB imagery using self-supervised vision transformer and convolutional decoder  
1210 trained on aerial lidar. *Remote Sensing of Environment*, 300, 113888.  
1211 <https://doi.org/10.1016/j.rse.2023.113888>

- 1212 Tompalski, P., White, J. C., Coops, N. C., & Wulder, M. A. (2019). Demonstrating the  
1213 transferability of forest inventory attribute models derived using airborne laser scanning  
1214 data. *Remote Sensing of Environment*, 227, 110–124.  
1215 <https://doi.org/https://doi.org/10.1016/j.rse.2019.04.006>
- 1216 Valbuena, R., O'Connor, B., Zellweger, F., Simonson, W., Vihervaara, P., Maltamo, M.,  
1217 Silva, C. A., Almeida, D. R. A., Danks, F., Morsdorf, F., Chirici, G., Lucas, R., Coomes,  
1218 D. A., & Coops, N. C. (2020). Standardizing Ecosystem Morphological Traits from 3D  
1219 Information Sources. *Trends in Ecology & Evolution*, 35(8), 656–667.  
1220 <https://doi.org/10.1016/j.tree.2020.03.006>
- 1221 Vincent, G., Verley, P., Brede, B., Delaitre, G., Maurent, E., Ball, J., Clocher, I., & Barbier, N.  
1222 (2023). Multi-sensor airborne lidar requires intercalibration for consistent estimation of  
1223 light attenuation and plant area density. *Remote Sensing of Environment*, 286, 113442.  
1224 <https://doi.org/https://doi.org/10.1016/j.rse.2022.113442>
- 1225 Wagner, F. H., Dalagnol, R., Carter, G., Hirye, M. C. M., Gill, S., Takougoum, L. B. S.,  
1226 Favrichon, S., Keller, M., Ometto, J. P. H. B., Alves, L., Creze, C., George-Chacon, S.  
1227 P., Li, S., Liu, Z., Mullissa, A., Yang, Y., Santos, E. G., Worden, S. R., Brandt, M., ...  
1228 Saatchi, S. (2025). *High Resolution Tree Height Mapping of the Amazon Forest using*  
1229 *Planet NICFI Images and LiDAR-Informed U-Net Model*.  
1230 <https://arxiv.org/abs/2501.10600>
- 1231 Wagner, F. H., Roberts, S., Ritz, A. L., Carter, G., Dalagnol, R., Favrichon, S., Hirye, M. C.  
1232 M., Brandt, M., Ciais, P., & Saatchi, S. (2024). Sub-meter tree height mapping of  
1233 California using aerial images and LiDAR-informed U-Net model. *Remote Sensing of*  
1234 *Environment*, 305, 114099. <https://doi.org/https://doi.org/10.1016/j.rse.2024.114099>
- 1235 Wedeux, B. M. M., & Coomes, D. A. (2015). Landscape-scale changes in forest canopy  
1236 structure across a partially logged tropical peat swamp. *Biogeosciences*, 12(22), 6707–  
1237 6719. <https://doi.org/10.5194/bg-12-6707-2015>
- 1238 Weinstein, B. G., Marconi, S., Bohlman, S. A., Zare, A., Singh, A., Graves, S. J., & White, E.  
1239 P. (2021). A remote sensing derived data set of 100 million individual tree crowns for  
1240 the national ecological observatory network. *ELife*, 10.  
1241 <https://doi.org/10.7554/eLife.62922>
- 1242 White, J. C., Chen, H., Woods, M. E., Low, B., & Nasonova, S. (2019). The Petawawa  
1243 Research Forest: Establishment of a remote sensing supersite. *The Forestry Chronicle*,  
1244 95(03), 149–156. <https://doi.org/10.5558/tfc2019-024>
- 1245 White, J. C., Coops, N. C., Wulder, M. A., Vastaranta, M., Hilker, T., & Tompalski, P. (2016).  
1246 Remote Sensing Technologies for Enhancing Forest Inventories: A Review. In  
1247 *Canadian Journal of Remote Sensing* (Vol. 42, Issue 5, pp. 619–641).  
1248 <https://doi.org/10.1080/07038992.2016.1207484>
- 1249 White, J. C., Tompalski, P., Bater, C. W., Wulder, M. A., Fortin, M., Hennigar, C., Robere-  
1250 McGugan, G., Sinclair, I., & White, R. (2025). Enhanced forest inventories in Canada:  
1251 implementation, status, and research needs. *Canadian Journal of Forest Research*, 55,  
1252 1–37. <https://doi.org/10.1139/cjfr-2024-0255>
- 1253 White, J. C., Tompalski, P., Coops, N. C., & Wulder, M. A. (2018). Comparison of airborne  
1254 laser scanning and digital stereo imagery for characterizing forest canopy gaps in  
1255 coastal temperate rainforests. *Remote Sensing of Environment*, 208, 1–14.  
1256 <https://doi.org/https://doi.org/10.1016/j.rse.2018.02.002>
- 1257 Wulder, M. A., White, J. C., Bater, C. W., Coops, N. C., Hopkinson, C., & Chen, G. (2012).  
1258 Lidar plots — a new large-area data collection option: context, concepts, and case

- 1259 study. *Canadian Journal of Remote Sensing*, 38(5), 600–618.  
1260 <https://doi.org/10.5589/m12-049>
- 1261 Wulder, M. A., White, J. C., Nelson, R. F., Næsset, E., Ørka, H. O., Coops, N. C., Hilker, T.,  
1262 Bater, C. W., & Gobakken, T. (2012). Lidar sampling for large-area forest  
1263 characterization: A review. *Remote Sensing of Environment*, 121, 196–209.  
1264 <https://doi.org/https://doi.org/10.1016/j.rse.2012.02.001>
- 1265 Xu, L., Saatchi, S. S., Shapiro, A., Meyer, V., Ferraz, A., Yang, Y., Bastin, J. F., Banks, N.,  
1266 Boeckx, P., Verbeeck, H., Lewis, S. L., Muanza, E. T., Bongwele, E., Kayembe, F.,  
1267 Mbenza, D., Kalau, L., Mukendi, F., Ilunga, F., & Ebuta, D. (2017). Spatial Distribution  
1268 of Carbon Stored in Forests of the Democratic Republic of Congo. *Scientific Reports*,  
1269 7(1), 15030. <https://doi.org/10.1038/s41598-017-15050-z>
- 1270 Yu, X., Hyyppä, J., Kaartinen, H., & Maltamo, M. (2004). Automatic detection of harvested  
1271 trees and determination of forest growth using airborne laser scanning. *Remote*  
1272 *Sensing of Environment*, 90(4), 451–462.  
1273 <https://doi.org/https://doi.org/10.1016/j.rse.2004.02.001>
- 1274 Zanne, A. E., Lopez-Gonzalez, G., Coomes, D. A., Ilic, J., Jansen, S., Lewis, S. L., Miller, R.  
1275 B., Swenson, N. G., Wiemann, M. C., & Chave, J. (2009). Data from: Global wood  
1276 density database. *Dryad Digital Repository*. <https://doi.org/10.5061/dryad.234>
- 1277 Zhang, B., Fischer, F. J., Coomes, D. A., & Jucker, T. (2023). Logging leaves a fingerprint on  
1278 the number, size, spatial configuration and geometry of tropical forest canopy gaps.  
1279 *Biotropica*, 55(2), 354–367. <https://doi.org/https://doi.org/10.1111/btp.13190>
- 1280 Zhang, B., Fischer, F. J., Prober, S. M., Yeoh, P. B., Gosper, C. R., Zdunic, K., & Jucker, T.  
1281 (2024). Robust retrieval of forest canopy structural attributes using multi-platform  
1282 airborne LiDAR. *Remote Sensing in Ecology and Conservation*, n/a(n/a).  
1283 <https://doi.org/https://doi.org/10.1002/rse2.398>

1284